CdL Scienza dei Materiali - Fisica delle Nanotecnologie - a.a. 2004/5

Appunti & trasparenze - Parte 8

Versione 3, Novembre 2004
Francesco Fuso, tel 0502214305, 0502214293 - fuso@df.unipi.it
http://www.df.unipi.it/~fuso/dida

Metodi ottici per l'osservazione e la realizzazione di nanostrutture: richiami sulla diffrazione, cenni di microscopia ottica, litografia ottica (maschere, resist, etching,…). Strategie per superare il limite di diffrazione: litografia UV, VUV e raggi-X, phase-shifting masks, etching anisotropo. Litografia atomica. Cenni su nanoimprinting

15/11/2004 – 11.30+1 ITI M
18/11/2004 – 9.30+1 ITI M

Introduzione: metodi ottici in micro- e nano-tecnologia

Obiettivi generali:

1. Sfruttare tecniche ottiche (radiazione visibile, UV) per produrre ("ritagliare") nanostrutture a partire da film sottili: **litografia ottica**;
2. Sfruttare le stesse tecniche per analizzare le nanostrutture: **microscopia ottica**

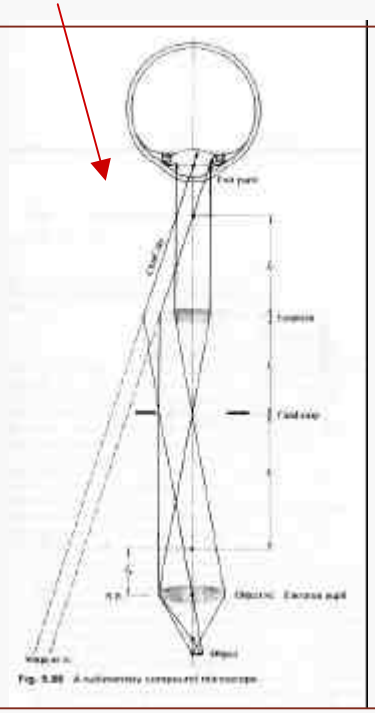

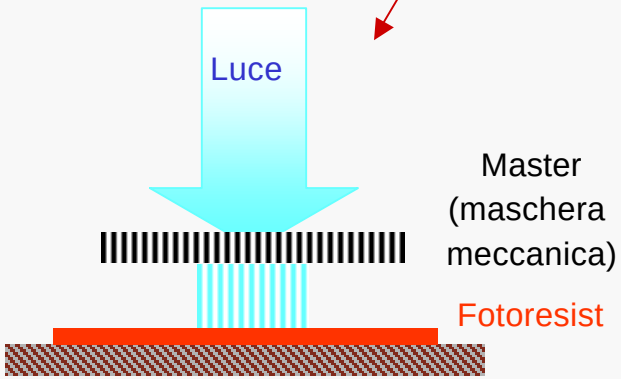

Problematica fondamentale:
la lunghezza d'onda può risultare "grande" rispetto alle dimensioni caratteristiche: fenomeno della **diffrazione ottica**

Da Hecht Zajac
Optics
Addison-Wesley (1974)

Richiami su interferenza e diffrazione

...al Coherent Oscillators

As a simple yet logical bridge between the studies of interference and diffraction, consider the arrangement of Fig. 10.6. The illustration depicts a linear array of N coherent point oscillators (or radiating antennas), which are each identical even to their polarization. For the moment, consider the oscillators to have no intrinsic phase difference, i.e. they each have the same epoch angle. The rays shown are all almost parallel, meeting at some very distant point P. If the spatial extent of the array is comparatively small, the separate wave amplitudes arriving at P will be essentially equal, having traveled nearly equal distances, that is

$$E_0(r_1) = E_0(r_2) = \cdots = E_0(r_N) = E_0(r).$$

The sum of the interfering spherical wavelets yields an electric field at P, given by the real part of

$$E = E_0(r)e^{i(kr_1 - \omega t)} + E_0(r)e^{i(kr_2 - \omega t)} + \cdots + E_0(r)e^{i(kr_N - \omega t)}. \tag{10.1}$$

It should be clear, from Section 9.1, that we need not be concerned with the vector nature of the electric field for this configuration. Now then

$$E = E_0(r)e^{-i\omega t}e^{ikr_1}[1 + e^{ik(r_2 - r_1)} + e^{ik(r_3 - r_1)} + \cdots + e^{ik(r_N - r_1)}].$$

The phase difference between adjacent sources is obtained from the expression $\delta = k_0\Lambda$ and since $\Lambda = nd \sin\theta$, in a medium of index n, $\delta = kd \sin\theta$. Making use of Fig. 10.6, it follows that $\delta = k(r_2 - r_1)$, $2\delta = k(r_3 - r_1)$ etc. Thus the field at P may be written as

$$E = E_0(r)e^{-i\omega t}e^{ikr_1}[1 + (e^{i\delta}) + (e^{i\delta})^2 + (e^{i\delta})^3 + \cdots (e^{i\delta})^{N-1}]. \tag{10.2}$$

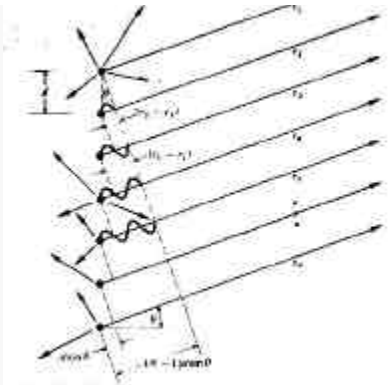

Fig. 10.6 A linear array of in-phase coherent oscillators. Note that at the angle shown $r_1 = r$ while at $\theta = 0$ it would be zero.

The bracketed geometric series has the value

$$(e^{i\delta N} - 1)/(e^{i\delta} - 1)$$

which can be rearranged into the form

$$\frac{e^{iN\delta/2}[e^{iN\delta/2} - e^{-iN\delta/2}]}{e^{i\delta/2}[e^{i\delta/2} - e^{-i\delta/2}]}$$

or equivalently

$$e^{i(N-1)\delta/2}\left[\frac{\sin N\delta/2}{\sin \delta/2}\right].$$

The field then becomes

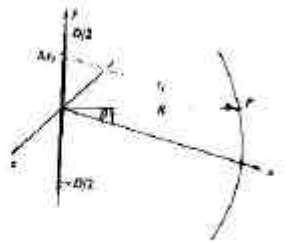

Fig. 10.8 A coherent line source.

$$E = E_0(r)e^{-i\omega t}e^{i(kr_1 + (N-1)\delta/2)}\left(\frac{\sin N\delta/2}{\sin \delta/2}\right). \tag{10.3}$$

Notice that if we define R to be the distance from the center of the line of oscillators to the point P, that is

$$R = \tfrac{1}{2}(N-1)d \sin\theta + r_1,$$

then Eq. (10.3) takes on the form

$$E = E_0(r)e^{i(kR - \omega t)}\left(\frac{\sin N\delta/2}{\sin \delta/2}\right). \tag{10.4}$$

Finally, then, the flux-density distribution within the diffraction pattern due to N coherent, identical, distant point sources in a linear array is proportional to $EE^*/2$ for complex E or

$$I = I_0\frac{\sin^2(N\delta/2)}{\sin^2(\delta/2)}, \tag{10.5}$$

where I_0 is the flux density from any single source arriving at P (see Problem 10.2 for a graphical derivation of the irradiance). For $N = 0$, $I = 0$, for $N = 1$, $I = I_0$, and for $N = 2$, $I = 4I_0\cos^2(\delta/2)$ in accord with Eq. (9.6). The functional dependence of I on θ is more apparent in the form

$$I = I_0\frac{\sin^2[N(kd/2)\sin\theta]}{\sin^2[(kd/2)\sin\theta]}. \tag{10.6}$$

The $\sin^2[N(kd/2)\sin\theta]$ term undergoes rapid fluctuations, while the function modulating it, $\{\sin[(kd/2)\sin\theta]\}^{-2}$, varies relatively slowly. The combined expression gives rise to a series of sharp principal peaks separated by small subsidiary maxima. The principal maxima occur in directions θ_m such that $\delta = 2m\pi$ where $m = 0, \pm1, \pm2, \ldots$. Because $\delta = kd\sin\theta$

$$d\sin\theta_m = m\lambda. \tag{10.7}$$

Since $[\sin^2 N\delta/2]/[\sin^2\delta/2] = N^2$ for $\delta = 2m\pi$ (from

Diffrazione di Fraunhofer

L'Hôspital's rule) the principal maxima have values $N^2 I_0$. This is to be expected inasmuch as all of the oscillators are in phase at that orientation. The system will radiate a maximum in a direction perpendicular to the array ($m = 0$, $\theta_0 = 0$ and π). As θ increases, δ increases and I falls off to zero at $N\delta/2 = \pi$, its first minimum. Note that if $d < \lambda$ in Eq. (10.7), only the $m = 0$ or zero-order principal maximum exists. *If we were looking at an idealized line source of electron-oscillators separated by atomic distances, we could expect only that one principal maximum in the light field.*

The antenna array of Fig. 10.7 can then transmit radiation in the narrow beam or lobe corresponding to a principal maximum (the parabolic dishes shown reflect into the forward direction and the radiation pattern is no longer symmetrical around the common axis.) Suppose that we have a system in which we can introduce an intrinsic phase shift of ε between adjacent oscillators. In that case

$$\delta = kd \sin\theta + \varepsilon;$$

the various principal maxima will occur at new angles

$$d \sin\theta_m = m\lambda - \varepsilon/k.$$

Concentrating on the central maximum $m = 0$, its orientation θ_m can be varied at will by merely adjusting the value of ε.

The principle of reversibility, which states that without absorption, wave motion is reversible, leads to the same field pattern for an antenna used as either a transmitter or receiver. The array, functioning as a radio telescope, can therefore be "pointed" by combining the output from the individual antennas with an appropriate phase shift, ε, introduced between each of them. For a given ε the output of the system corresponds to the signal impinging on the array from a specific direction in space.

Figure 10.7 is a photograph of the first multiple radio interferometer designed by W. N. Christiansen and built in Australia in 1951. It consists of 32 parabolic antennas, each 2 m in diameter, designed to function in phase at the wavelength of the 21 cm hydrogen emission line. The antennas are arranged along an east–west baseline with 7 m separating each one. This particular array utilizes the earth's rotation as the scanning mechanism.

Examine Fig. 10.8 which depicts an idealized line source of electron-oscillators (e.g., the secondary sources of the Huygens–Fresnel principle for a long slit whose width is much less than λ illuminated by plane waves). Each point emits a spherical wavelet which we write as

$$E = \left(\frac{\mathcal{E}_0}{r}\right) \sin(\omega t - kr)$$

explicitly indicating the inverse r-dependence of the amplitude. The quantity $\mathcal{E}_0$ is said to be the *source strength*. The present situation is distinct from that of Fig. 10.6 in that now the sources are very weak, their number, N, is tremendously large and the separation between them vanishingly small. A minute, but finite segment of the array Δy_i, will contain $\Delta y_i(N/D)$ sources where D is the entire length of the array. Imagine then that the array is divided up into M such segments, i.e., i goes from 1 to M. The contribution to the electric field intensity at P from the ith segment is accordingly

$$E_i = \left(\frac{\mathcal{E}_0}{r_i}\right) \sin(\omega t - kr_i) \left(\frac{N\Delta y_i}{D}\right)$$

provided that Δy_i is so small that the oscillators within it have a negligible relative phase difference (r_i = constant) and their fields simply add constructively. We can cause the array to become a continuous (coherent) line source by letting N approach infinity. This description, besides being fairly realistic on a macroscopic scale, also allows the use of the calculus for more complicated geometries. Certainly as N approaches infinity, the source strengths of the individual oscillators must diminish to near zero if the total output is to be finite. We can therefore define a constant $\mathcal{E}_L$ as the *source strength per unit length* of the array, that is

$$\mathcal{E}_L \equiv \frac{1}{D} \lim_{\substack{N\to\infty \\ \Delta y_i \to 0}} (\mathcal{E}_0 N). \tag{10.8}$$

The net field at P from all M segments is

$$E = \sum_{i=1}^{M} \frac{\mathcal{E}_L}{r_i} \sin(\omega t - kr_i)\, \Delta y_i.$$

For a continuous line source Δy_i can become infinitesimal ($M \to \infty$) and the summation is then transformed into a definite integral

$$E = \mathcal{E}_L \int_{-D/2}^{+D/2} \frac{\sin(\omega t - kr)}{r}\, dy, \tag{10.9}$$

where $r = r(y)$. The approximations used to evaluate Eq. (10.9) must depend on the position of P with respect to the array and will therefore make the distinction between Fraunhofer and Fresnel diffraction. The coherent *optical* line source does not now exist as a physical entity but we will make good use of it as a mathematical device.

10.2 FRAUNHOFER DIFFRACTION

10.2.1 The Single Slit

Return to Fig. 10.8 where now the point of observation is very distant from the coherent line source and $R \gg D$. Under these circumstances $r(y)$ never deviates appreciably from its midpoint value R so that the quantity $(\mathcal{E}_L/R)$ at P is essentially constant for all elements dy. It follows from Eq. (10.9) that the field at P due to the differential segment of the source dy is

$$dE = \frac{\mathcal{E}_L}{R} \sin(\omega t - kr)\, dy, \tag{10.10}$$

where $(\mathcal{E}_L/R)\, dy$ is the amplitude of the wave. Notice that the phase is very much more sensitive to variations in $r(y)$ than is the amplitude so that we will have to be more careful about introducing approximations into it. We can expand $r(y)$, in precisely the same manner as was done in Problem (9.4), to get it as an explicit function of y, thus

$$r = R - y \sin\theta + (y^2/2R) \cos^2\theta + \cdots, \tag{10.11}$$

where θ is measured from the xz-plane. The third term can be ignored so long as its contribution to the phase is insignificant even when $y = \pm D/2$, i.e. $(\pi D^2/4\lambda R) \cos^2\theta$ must be negligible. This will be true for all values of θ when R is adequately large and we again have the Fraunhofer condition. The distance r is then linear in y. Substituting into Eq. (10.10) and integrating leads to

$$E = \frac{\mathcal{E}_L}{R} \int_{-D/2}^{+D/2} \sin[\omega t - k(R - y \sin\theta)]\, dy, \tag{10.12}$$

and finally

$$E = \frac{\mathcal{E}_L D}{R} \frac{\sin[(kD/2)\sin\theta]}{(kD/2)\sin\theta} \sin(\omega t - kR). \tag{10.13}$$

To simplify the appearance of things let

$$\beta \equiv (kD/2) \sin\theta \tag{10.14}$$

so that

$$E = \frac{\mathcal{E}_L D}{R} \left(\frac{\sin\beta}{\beta}\right) \sin(\omega t - kR). \tag{10.15}$$

The quantity most readily measured is the irradiance (forgetting the constants) $I(\theta) = \langle E^2 \rangle$ or

$$I(\theta) = \frac{1}{2} \left(\frac{\mathcal{E}_L D}{R}\right)^2 \left(\frac{\sin\beta}{\beta}\right)^2, \tag{10.16}$$

where $\langle \sin^2(\omega t - kR) \rangle = \frac{1}{2}$. When $\theta = 0$, $\sin\beta/\beta = 1$ and $I(\theta) = I(0)$ which corresponds to the *principal maximum*. *The irradiance resulting from an idealized coherent line source in the Fraunhofer approximation* is then

$$I(\theta) = I(0) \left(\frac{\sin\beta}{\beta}\right)^2, \tag{10.17}$$

or using the *sinc function* (Section 7.9 and Table 1 of the Appendix)

$$I(\theta) = I(0) \operatorname{sinc}^2 \beta.$$

There is symmetry about the y-axis and this expression holds for θ measured in any plane containing that axis.

Diffrazione ottica

Limite ultimo nella risoluzione spaziale dei metodi ottici:
fenomeno della diffrazione

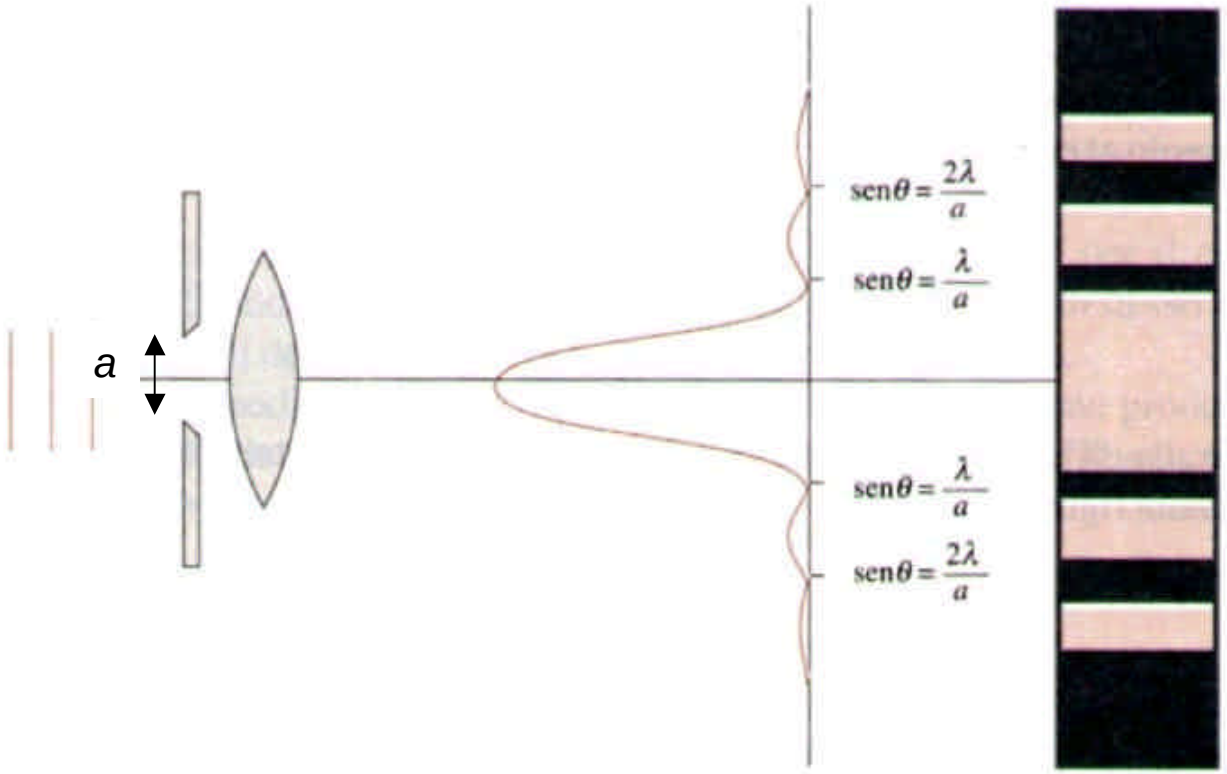

"Cono di diffusione":
$\sin\theta \sim \lambda/a$

Intensità diffratta:
$I \sim I_0 (\sin\alpha/\alpha)^2$
con:
$\alpha = \pi\, a \sin\theta / \lambda$

La diffrazione da un sistema ottico con apertura numerica NA limita la risoluzione spaziale ad un valore ~ 0.6 λ/NA
(limite di Abbe)

Criteri per la risoluzione spaziale

Da Brandon Kaplan
Microstruct. Charact.
of Materials
Wiley (1999)

3.1.2.1 POINT-SOURCE ABBE IMAGE

The calculated intensity distribution assumes a parallel beam of light travelling along the axis of a thin lens and brought to a focus at the focal distance (Fig. 3.8). For the *cylindrically symmetric* case, the ratio of the peak intensities for the primary and secondary peaks in the intensity distribution is *ca* 9 : 1, while the width of the primary peak is given by the *Abbe equation* as follows:

Abbe

$$\delta = 0.61 \frac{\lambda}{\mu \sin \alpha} \qquad (3.1)$$

where λ is the wavelength of the radiation, α is the aperture (half-angle) of the lens (determined by the ratio of the lens radius to its focal length), and μ is the refractive index of the medium between the lens and the focal point ($\mu \approx 1$ for air).

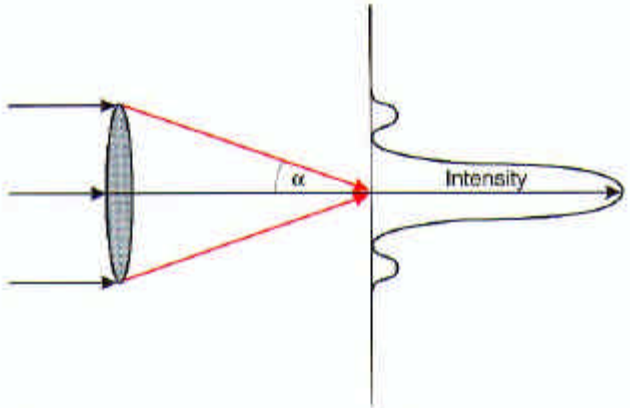

Figure 3.8 The Abbe equation gives the width of the first intensity peak for the image of point object at infinity in terms of the angular aperture of the lens α and the wavelength of t radiation λ

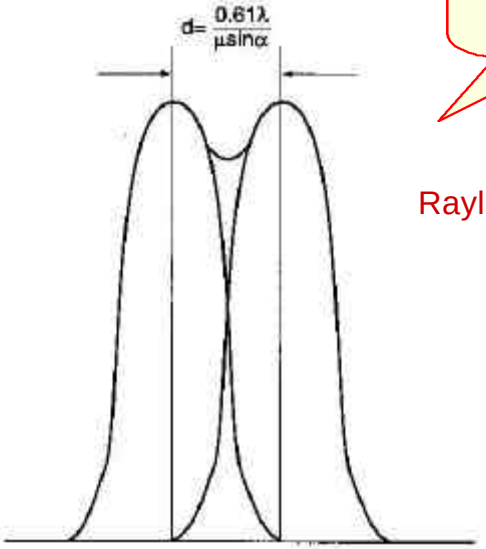

Rayleigh

Figure 3.10 The Raleigh resolution criterion requires that two point sources at infinity have an angular separation which is sufficient to place the maximum intensity of the primary image peak of one source at the position of the first minimum of the second

Criteri di risoluzione validi sia per microscopia che per litografia (per “reciprocità”)

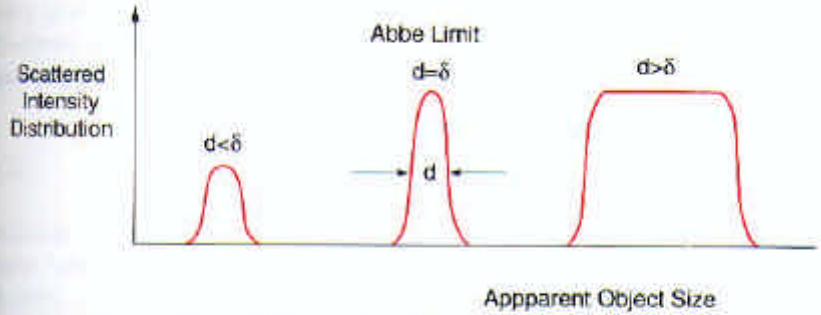

Figure 3.11 Large objects of diameter d are blurred by the diffraction limit δ derived from the Abbe relationship, but objects smaller than the Abbe width are still detectable in the microscope, although the intensity is reduced and they have an apparent width given by the Abbe equation

Microscopia ottica

Da Hecht Zajac
Optics
Addison-Wesley (1974)

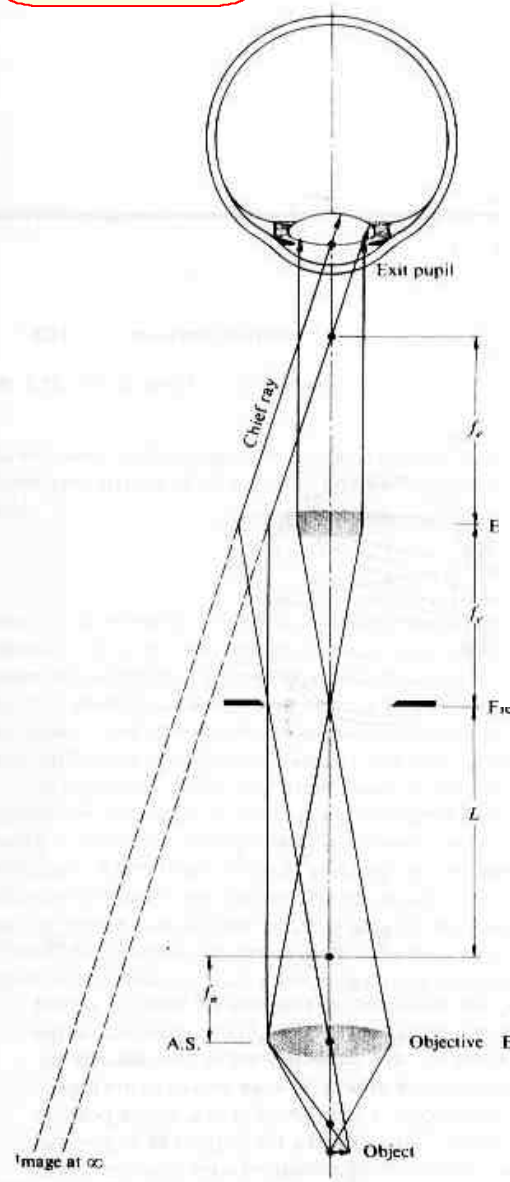

Fig. 5.86 A rudimentary compound microscope.

the magnifying power of the entire system is the product of the transverse linear magnification of the objective, M_{T_o}, and the angular magnification of the eyepiece, M_{A_e}, that is

$$\text{M.P.} = M_{T_o} M_{A_e} \tag{5.70}$$

Recall that $M_T = -x_i/f_o$ (5.26), and with this in mind most, but not all, manufacturers design their microscopes such that the distance (corresponding to x_i) from the second focus of the objective to the first focus of the eyepiece is standardized at 160 mm. This distance, known as the *tube length*, is denoted by L in the figure. (Some authors define tube length as the image distance of the objective.) Hence, with the final image at infinity and the standard near point taken as 10 inches or 254 mm

$$\text{M.P.} = \left(-\frac{160}{f_o}\right)\left(\frac{254}{f_e}\right) \tag{5.71}$$

and the image is inverted (M.P. < 0). Accordingly, the barrel of an objective with a focal length f_o of say 32 mm will be engraved with the markings 5× (or ×5) indicating a power of 5. Combined with a 10× eyepiece (f_e = 1 inch) the microscope M.P. would then be 50×.

Microscopio:
obiettivo+oculare (+…)

Da Brandon Kaplan
Microstruct. Charact.
of Materials
Wiley (1999)

Profondità di campo

3 Depth of Field and Depth of Focus

…e the resolution available for an object in focus in the image plane is limited by numerical aperture of the objective lens, it follows that the object need not be at exact object distance from the lens u, but may be displaced from this plane …out sacrificing any resolution (Fig. 3.12). The distance over which the object …ains in focus is defined as the *depth of field*,

$$d = \delta \tan\alpha \tag{3.2}$$

…re 3.12 Since the resolution is finite, the object need not be in the exact object-plane …tion in order to remain in focus, and there is an allowed depth of field d. Similarly, the …e may be observed without loss of resolution if the image plane is slightly displaced, so there is an allowed depth of focus D

where α is half the angle subtended by the objective aperture at the focal point. Similarly, the image will remain in focus if it is displaced from its geometrically defined position at a distance v from the lens. The distance over which the image remains in focus is termed the *depth of focus*, as follows:

$$D = M^2 d \tag{3.3}$$

where M is the magnification. (Both of these expressions (equations (3.2) and (3.3)) are approximate and assume that the objective can be treated as a 'thin lens', which is never the case in a commercial instrument.) Since the resolution is given by $\delta = 0.61\lambda/\mu \sin\alpha = 0.61\lambda/NA$, it follows that the depth of field decreases as the numerical aperture increases. For the highest image resolution, the specimen should be positioned to an accuracy of better than 0.5 µm, which determines the required mechanical stability of the specimen stage.

The depth of focus is considerably less critical. Bearing in mind that a magnification of the order of 100 is necessary if all of the resolved detail is to be recorded, displacements of the order a millimetre are acceptable.

Limite diffrazione invalicabile
(ma esistono strategie per aumentare contrasto)

Microscopia ottica confocale

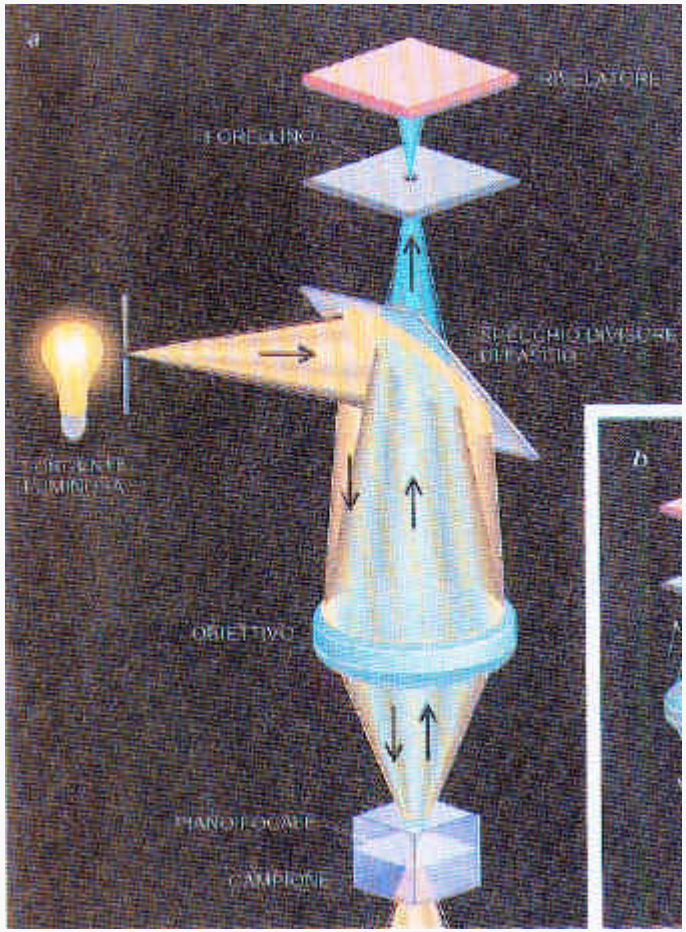

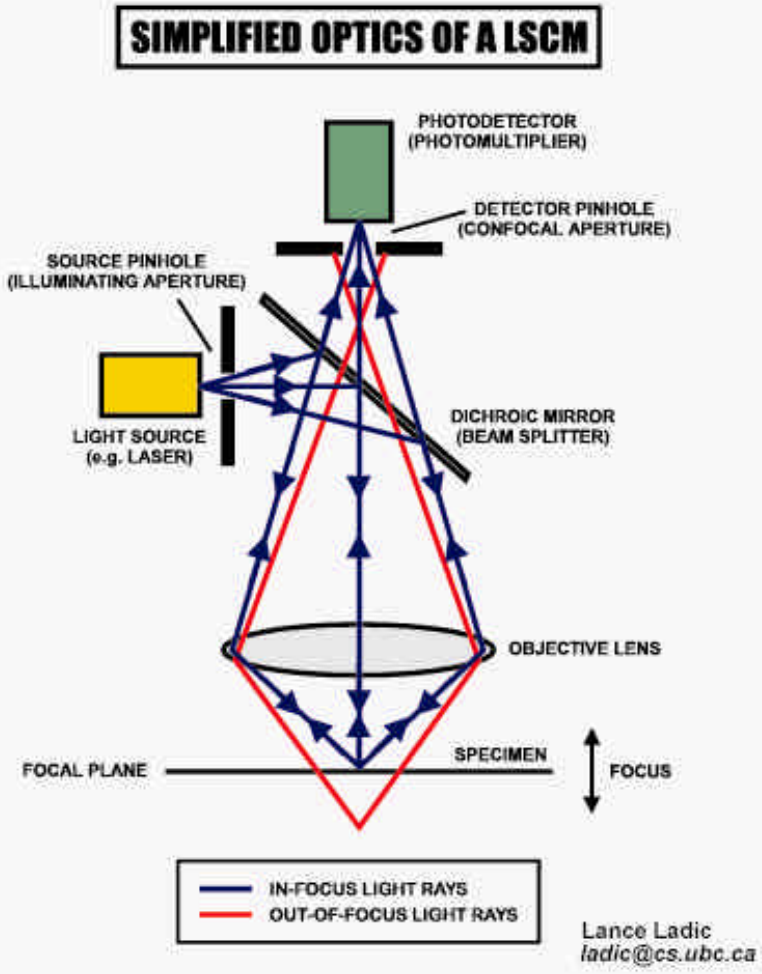

I microscopi confocali, precursori del microscopio con eccitazione a due fotoni per la visualizzazione tridimensionale di strutture biologiche, permettono di osservare ad alta risoluzione un singolo piano di un campione. Innanzitutto, la luce (*giallo in a*) viene focalizzata con un obiettivo in un fascio a forma di clessidra, in modo che la porzione più ristretta del fascio colpisca una piccola regione del campione alla profondità desiderata. Quindi la luce riflessa da quella regione (*blu*) viene focalizzata in un punto e fatta passare attraverso un forellino in una maschera posta davanti al rivelatore.

Nello stesso tempo la maschera blocca la maggior parte della luce riflessa dalle parti del campione che si trovano sopra (*rosso in b*) e sotto (*arancione*) il piano prescelto. Infine, la luce viene fatta scorrere rapidamente sul campione fino a che non viene analizzato l'intero piano. Per rendere più veloce il procedimento di scansione, alcuni microscopi confocali sono dotati di un disco che contiene centinaia di forellini, attraverso i quali viene inviata e raccolta la luce (*c*). Il disco ruota per garantire che nella scansione venga coperto ogni punto del piano.

Laser Scanning Confocal Micr.
--> risoluzione dipende
da focalizz. laser (0.5 µm)

Applicazioni confocale: solid-state e biophysics

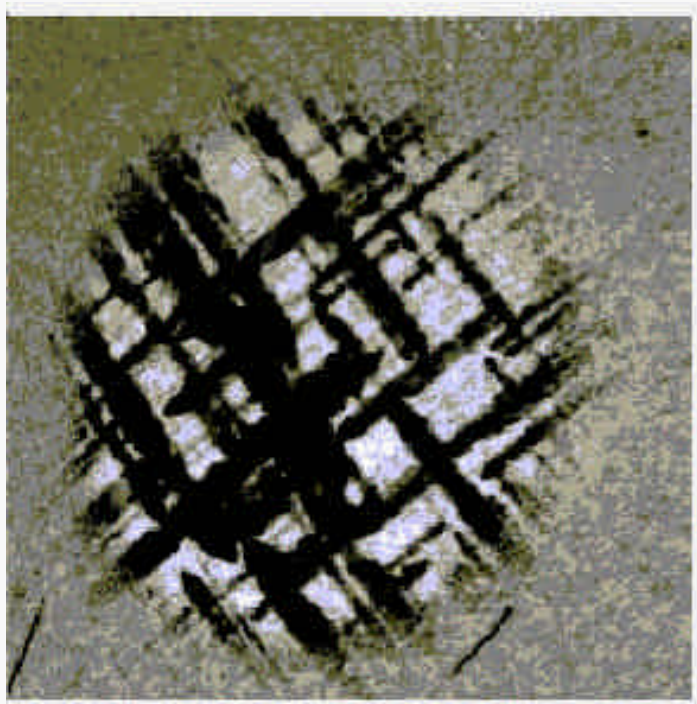

Confocal photoluminescence images of a II-VI laser structure sh
ZnCdSe/ZnSSe/ZnMgSSe separate confinement heterostructure:

"Degradazione' di eterostrutture

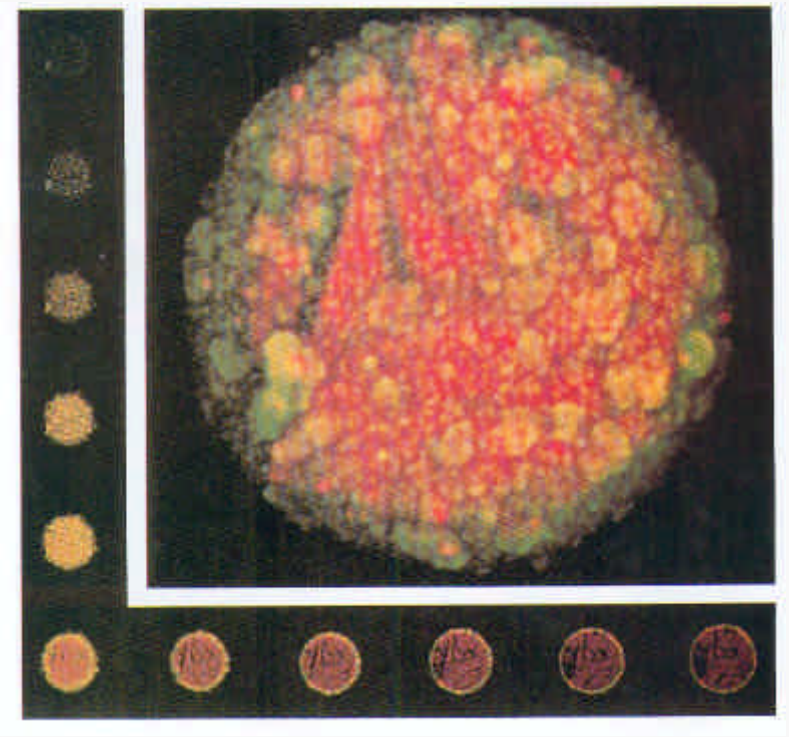

Microcapsula di fluido con **cromofori**

Confocale: possibilità mappatura "3D"
(per campioni luminescenti o con cromofori)
con alta risoluzione spaziale

Definizione litografica di strutture

Generalmente l'obiettivo è definire lateralmente delle strutture per realizzare un dispositivo, cioè creare un *pattern* con risoluzione spaziale pari alla dimensione laterale minima delle strutture desiderate (dal µm degli anni '80 a sotto i 100 nm per i prossimi anni)

Generalmente tecniche di tipo top-down (cioè rimozione localizzata di zone di film,…)

Tecnica maggiormente diffusa: litografia ottica (e con fasci di cariche)

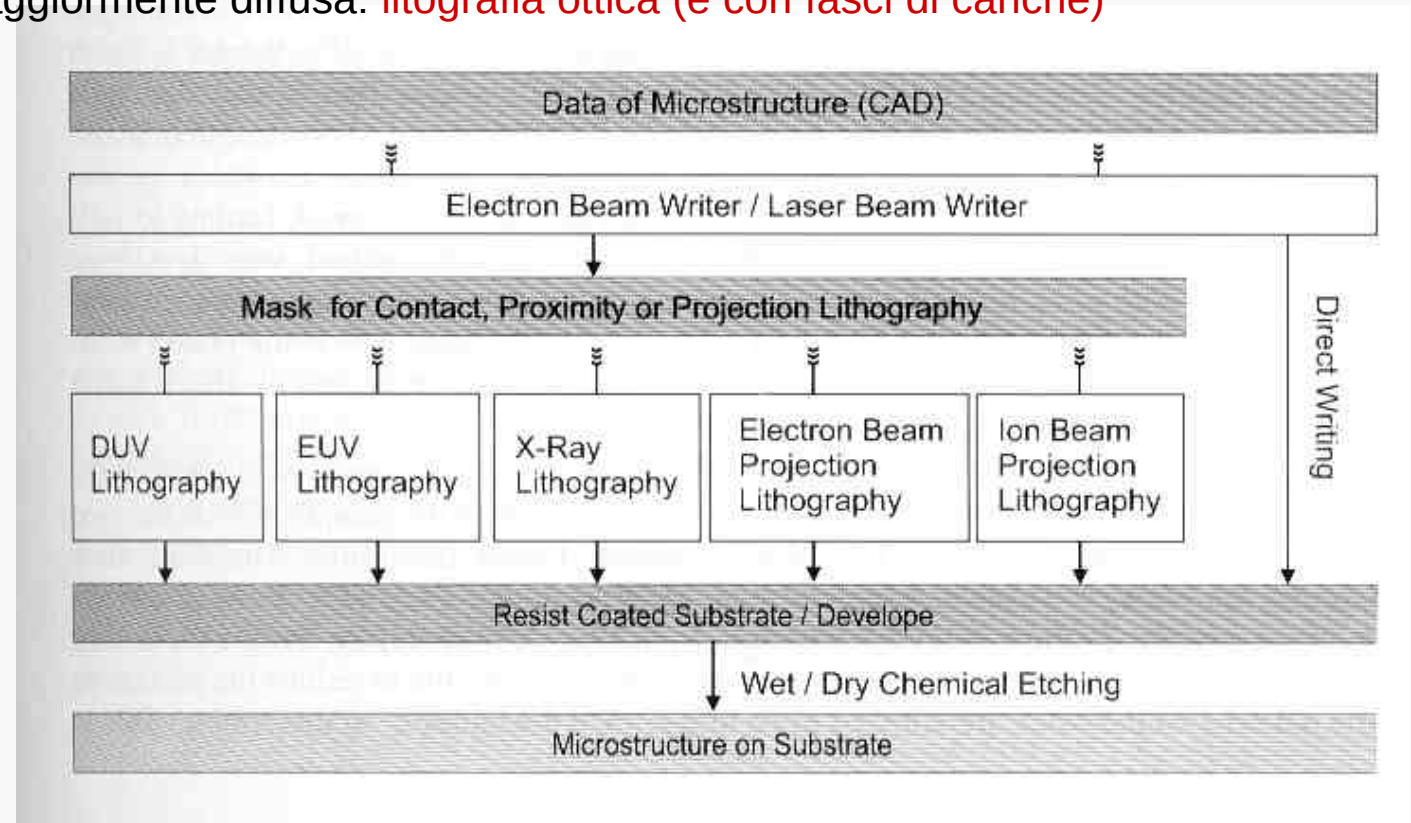

Litografia ottica

Ingredienti litografia ottica:
- radiazione e.m. (ben collimata!)
- maschera meccanica (trasp/opaca)
- fotoresist (ben depositato!)
- sviluppo ed etching

Vantaggi “evidenti” litografia ottica:
- flessibilità
- semplicità
- “parallelismo” di processo
- scalabilità

Risoluzione spaziale finale dipende da diversi fattori:
Lunghezza d’onda, qualità fotoresist, processo di etching, etc.

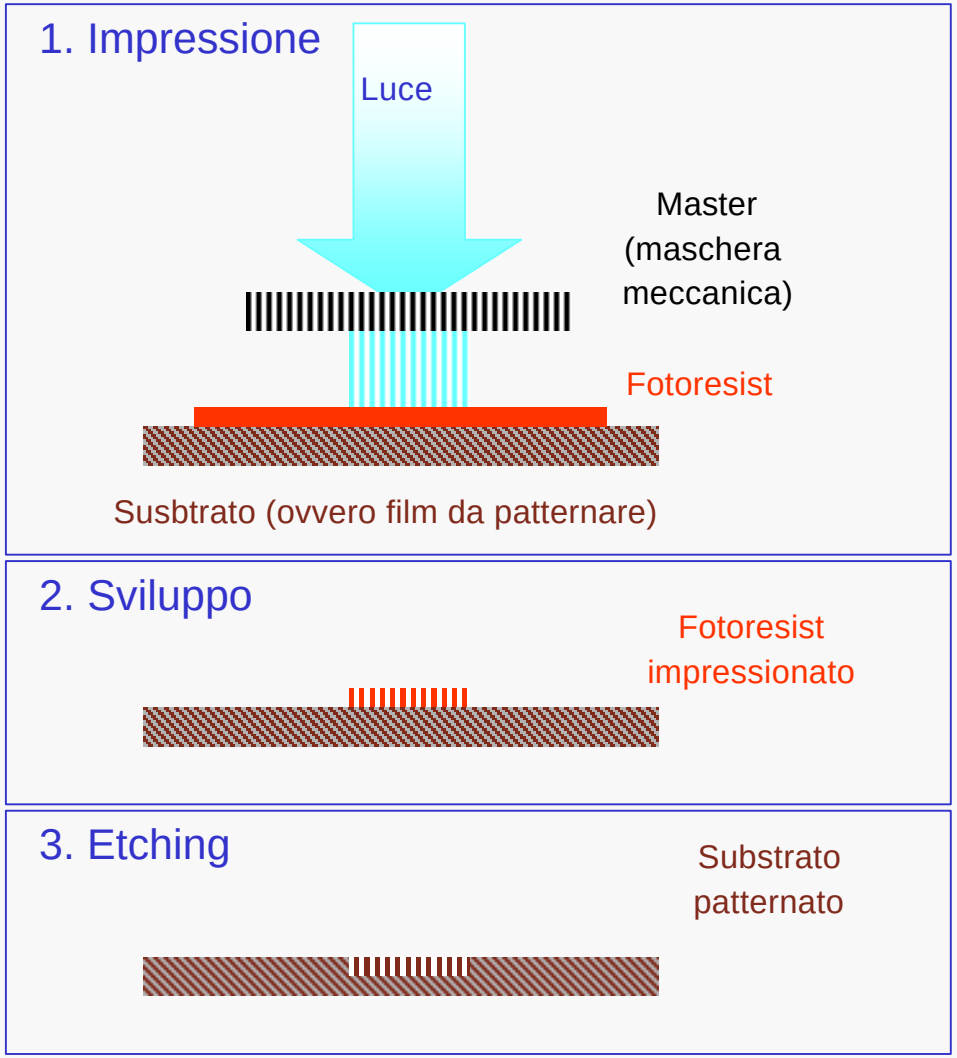

Configurazioni maschera

Contatto:
buona definizione
ma problemi “chimici”
e durata della maschera

Prossimità:
elimina problemi
maschera ma
sensibile a diffusione
luce (occorre collimare)

Proiezione:
maggiore versatilità,
minore dipendenza da
qualità maschera, ma
dipende da qualità
del sistema ottico
(il sistema più usato,
generalmente con
ingrandimento <1,
assieme a step-and-repeat
per grosse superfici)

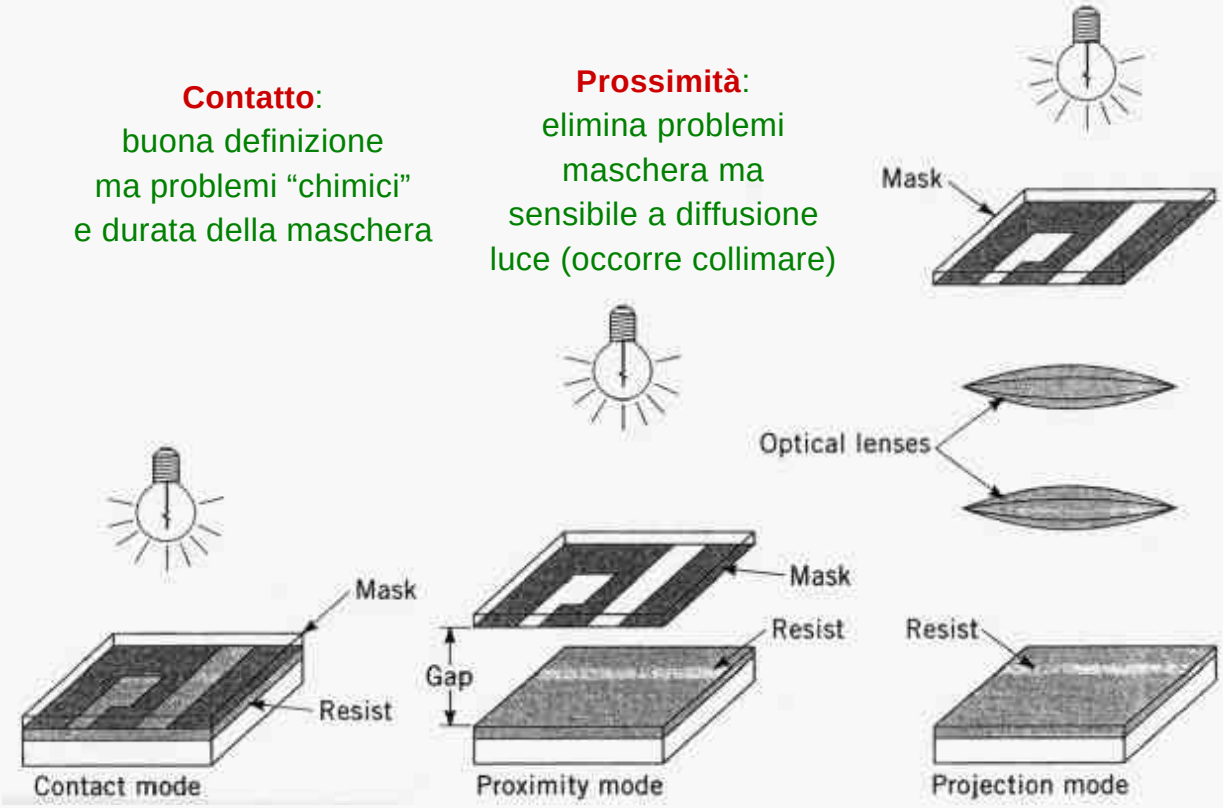

Master (maschere) possono essere prodotte con altre tecniche e replicate con litografia ottica

Pattern complessi possono essere prodotti con un’unica esposizione su superfici relativamente ampie (> mm^2)

Materiale parzialemente tratto dal seminario di Michele Alderighi (giu. 2002)

Fotoresist I

Da M. Madou,
Fundamentals of microfab.,
CRC (1997)

Requisiti fondamentali fotoresist:
- buono sticking al substrato
- omogeneità e spessore uniforme
- efficiente modifica solubilità quando impressionato dalla luce (typ. UV)
- buona sensibilità alla radiazione
- deve riprodurre fedelmente il pattern

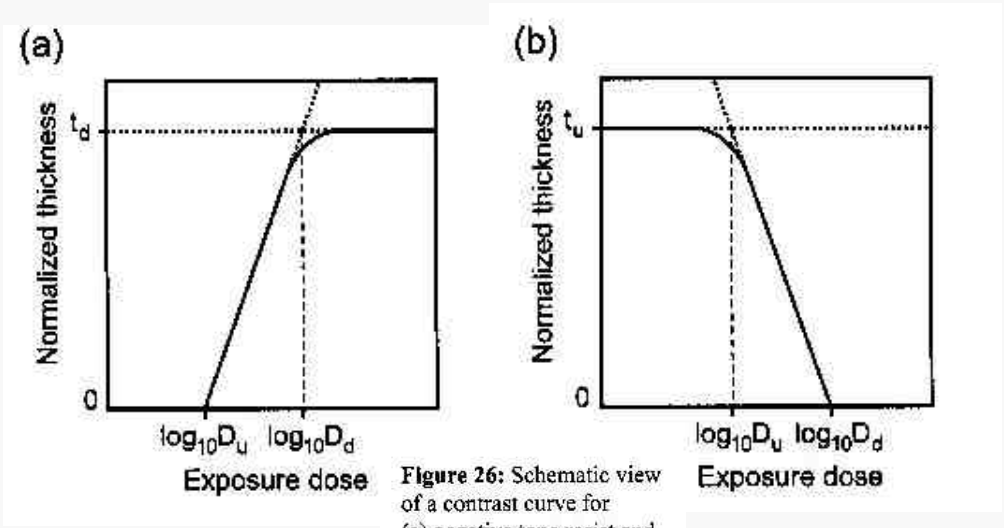

Figure 26: Schematic view of a contrast curve for (a) negative tone resist and (b) positive tone resist.

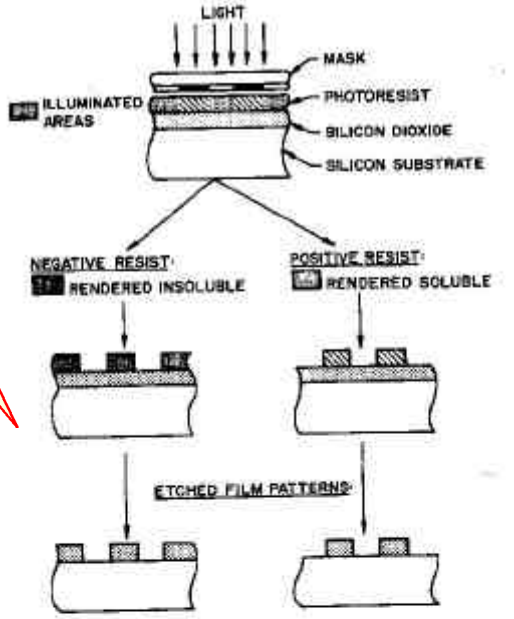

negativi positivi

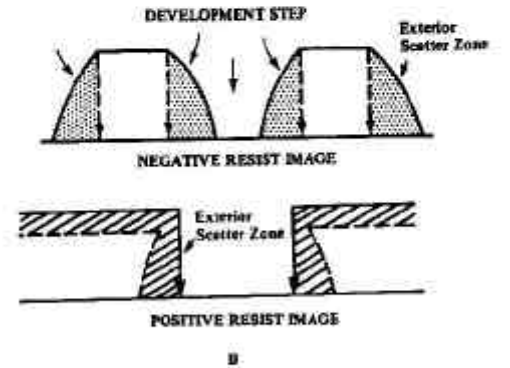

Figure 1.1 Positive and negative resist exposure, development, and edge-scattered radiation. (A) Positive and negative resists, exposure, and development. Positive resists develop in the exposed region and usually remain soluble for lift-off. Negative resists remain in the exposed region but are insoluble and not suitable for lift-off (see text). (B) Edge-scattered radiation profile for negative and positive resists. Time-independent development of cross-linked negative resist fails to remove light scatter zone. Development of positive resist rapidly removes exposed region and can be quenched to inhibit removal of lateral scattered exposed resist region. (From Brodie, I. and J. J. Muray, The Physics of Microfabrication, Plenum Press, New York, 1982. With permission.)

"Sensibilità":
N = numero scissioni legami = G*dose/100
con dose di energia in eV, e G_{typ} ~ 1-10

Fotoresist II

7 Photoresist

Photoresists are also an integral part of lithography. The performance of the resist is the determining factor for the magnitude of the technology factor k_1. In general, photoresists are polymers which react when exposed to light. There are two different types of resists: With positive tone resists, the exposed areas of the resist will dissolve in the developer, with negative tone resists, the exposed areas will remain.

Positive tone resists consist of three components, a resin, which serves as a binder and establishes the mechanical properties, a photoactive compound (PAC), and a solvent to keep the resist liquid. The resin is not normally responsive to the exposure. The commonly used positive tone resist system for g- and i-line lithography is the novolac/diazonaphthoquinones (DNQ) system. The novolac is the resin material and dissolves in aqueous bases. The DNQ is the PAC, but when unexposed it acts as a dissolution inhibitor. Figure 22 shows the reaction cycle of the DNQ upon exposure. Upon exposure N_2 is split off the molecule. After a rearrangement, the molecule undergoes a reaction with the H_2O, which stems from the air. The reaction product now does not behave as a dissolution inhibitor, but as a dissolution enhancer. Therefore the exposed areas of the resist will dissolve about 100 times quicker than the unexposed areas.

Negative tone resists also consist of the three compounds: resin, photoactive compound and a solvent to keep the resist liquid. The resin consists of a cyclic synthetic rubber, which is not radiation-sensitive, but strongly soluble in the developer (non-polar organic solvents). The PAC is normally a bis-arylazide. Figure 23 shows the chemical structure of a rubber resin and a PAC. Upon exposure, the PAC dissociates into *nitrene* and N_2. These nitrene molecules are able to react with the rubber molecules, so a cross-linking between two rubber molecules can be established. Thus a three-dimesional cross-linked molecular network is formed, which is insoluble in the developer .

As device dimensions are scaled down further, the g-line steppers as well as the novolac/DNQ resists have been improved, so the features for 350 nm generation could be printed. But reaching the 250 nm generation, the illumination wavelength was shifted to 250 nm, too. However, at this wavelength novolac and DNQ do strongly absorb the light, therefore another class of resists had to be developed. Furthermore, the intensity of

Positive resist

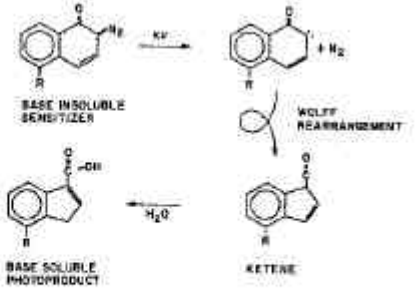

Figure 22: Exposure process of positive tone DNQ-resists [34], [39].

Negative resist

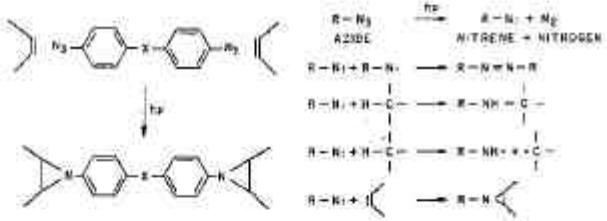

Figure 23: Reaction cycle of a negative tone resist during exposure [34], [39].

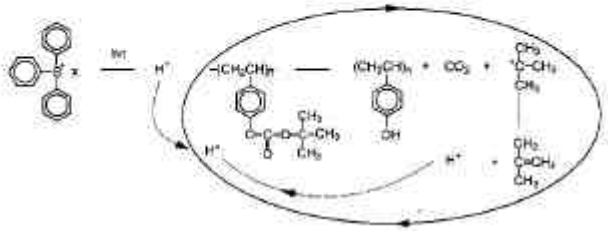

Figure 24: Chemical amplification cycle in a CAR [40].

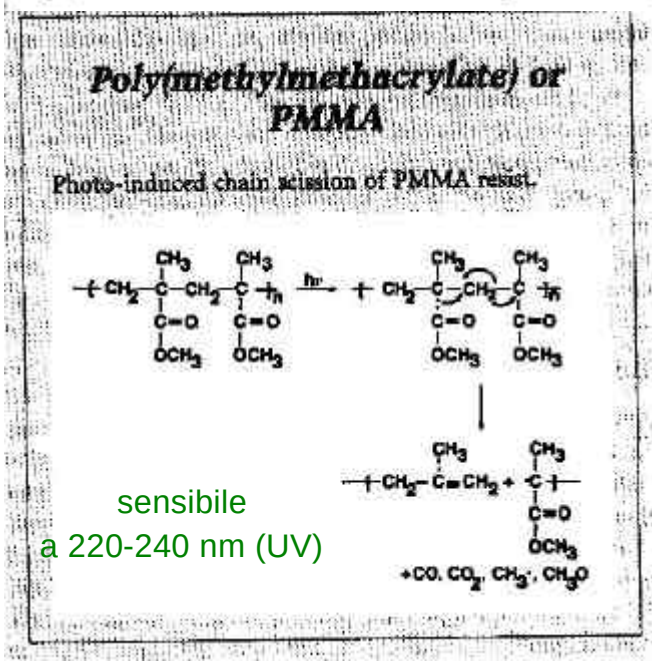

sensibile
a 220-240 nm (UV)

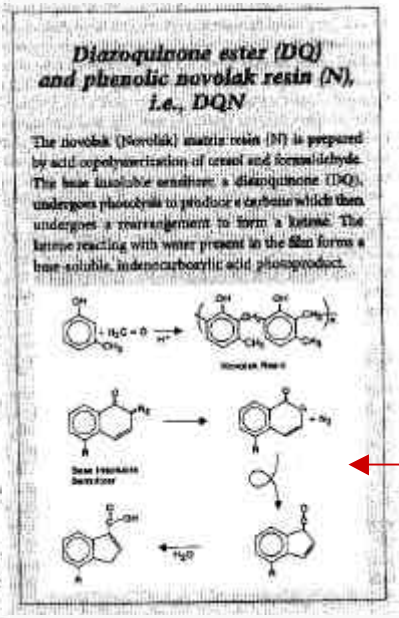

Esempi di fotoresist positivi (sviluppo es. KOH o acqua)

sensibile
a 365 nm (Hg-lamps)

Deposizione fotoresist

Deposizione usata più frequentemente: **spin-coating** (buona per polimeri)
(altrimenti spray, elettroforesi, Langmuir-Blodgett deposition, dipping per SAMs, …)

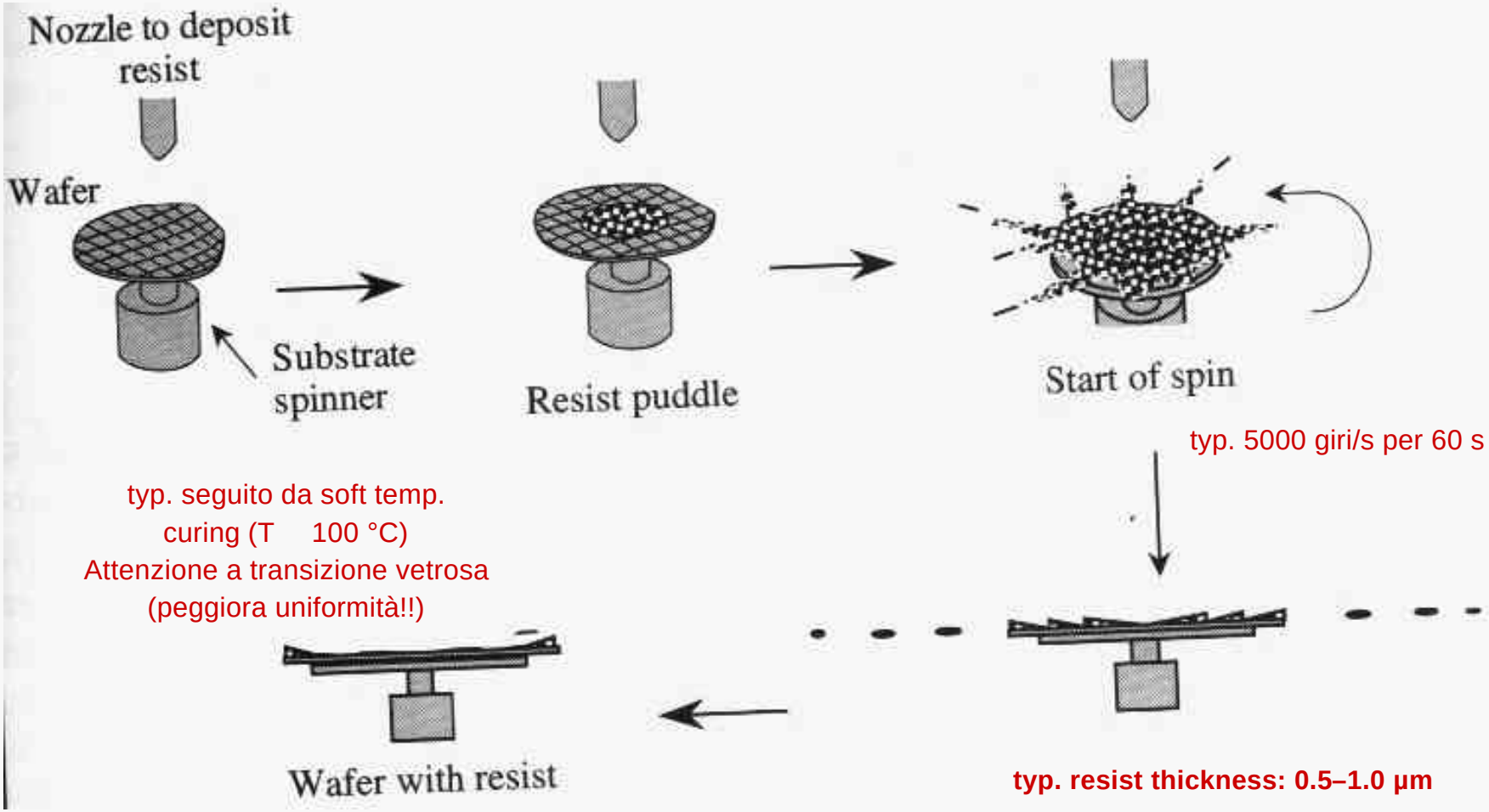

Spin-coating: ottima omogeneità, rapidità, semplicità

Etching

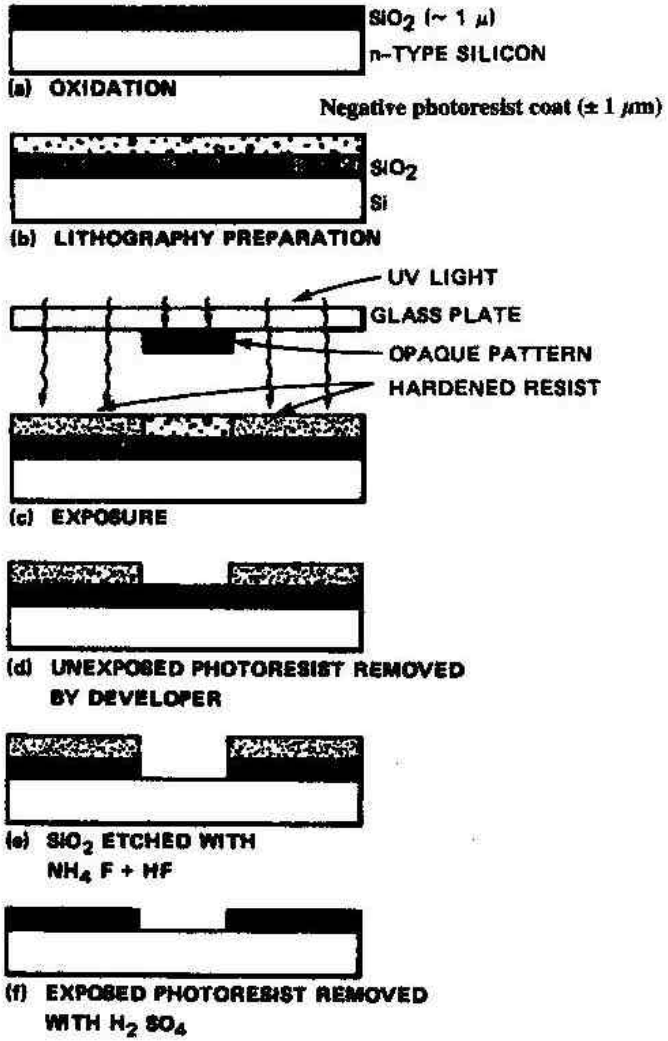

Figure 1.22 Basic IC process steps on an oxidized Si wafer; photolithography (with a negative-tone resist), including exposure, development, oxide etching, and resist stripping. (From Brodie. I. and J. J. Muray, The Physics of Microfabrication, Plenum Press, New York, 1991. With permission.)

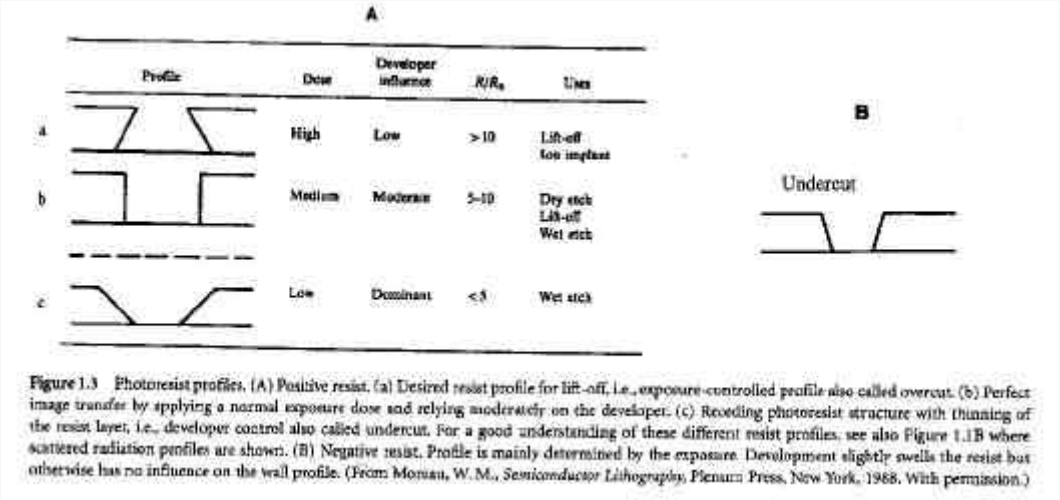

Figure 1.3 Photoresist profiles. (A) Positive resist. (a) Desired resist profile for lift-off, i.e., exposure-controlled profile also called overcut. (b) Perfect image transfer by applying a normal exposure dose and relying moderately on the developer. (c) Receding photoresist structure with thinning of the resist layer, i.e., developer control also called undercut. For a good understanding of these different resist profiles, see also Figure 1.1B where scattered radiation profiles are shown. (B) Negative resist. Profile is mainly determined by the exposure. Development slightly swells the resist but otherwise has no influence on the wall profile. (From Moreau, W. M., *Semiconductor Lithography*, Plenum Press, New York, 1988. With permission.)

Etching del resist può essere “wet”
(typ. attacco acido da fase liquida)
o “dry” (typ. con plasma ossidante”)

Etching deve essere seguito
da fase di “stripping”,
a volte con
“lift-off” del resist non impressionato

Importanza ruolo dei “dettagli” dell’esposizione
(overcut/undercut)

Risoluzione spaziale I

Da M. Madou, Fundamentals of microfab., CRC (1997)

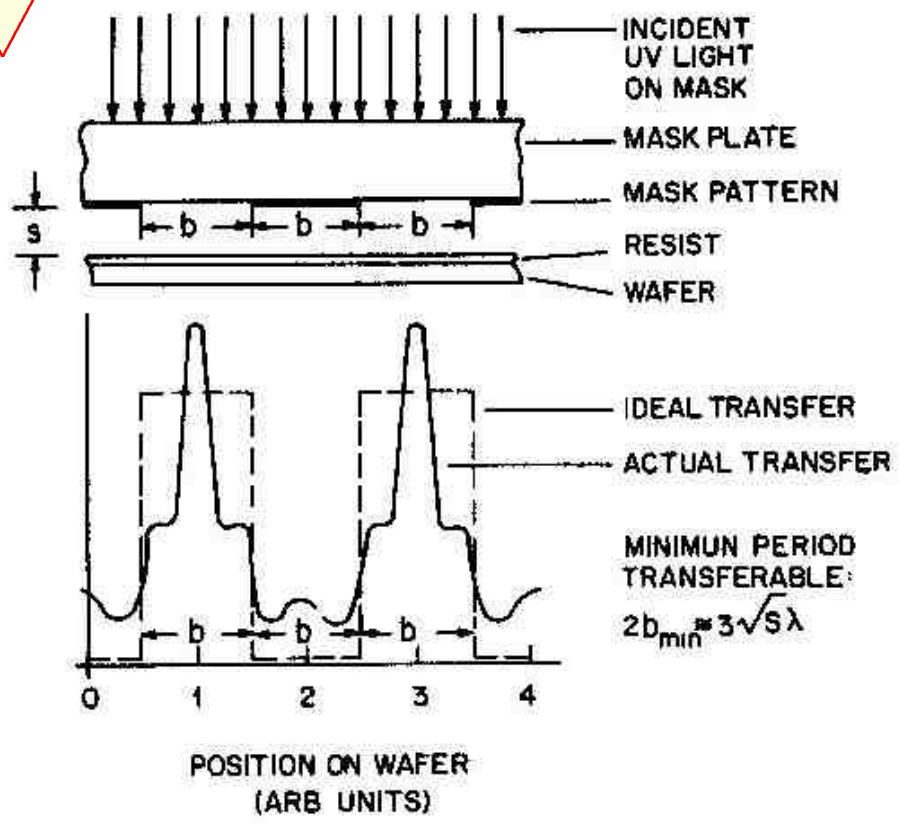

Figure 1.7 Light distribution profiles on a photoresist surface after light passed through a mask containing an equal line and space grating. (From Willson, C. G., in *Introduction to Microlithography*, Thompson, L. F., Willson, C. G., and Bowden, M. J., Eds., American Chemical Society, Washington, D.C., 1994. With permission.)

Ulteriori limitazioni alla risoluzione sono dovuti a distanza mask/resist e spessore resist (per effetto di "profondità di campo"

Formula semi-empirica:

$$2b_{min} = 3\sqrt{\lambda\left(s + \frac{Z}{2}\right)} \qquad 1.12$$

where b_{min} stands for half the grating period, s for the gap between the mask and the photoresist surface, λ for the wavelength of the exposing radiation, and z for the photoresist thickness.

Esempio:

λ = 350 nm, s = 5 µm, Z = 0.5 µm

--> b_{min} > 2 µm!!!

Importanza parametri s e Z

Risoluzione spaziale II

2 Optical Lithography

Optical lithography is the most important type of lithography. Originally the name referred to lithography using light with wavelength in the visible range. Nevertheless, gradually, the wavelength was driven down to 193 nm, which is used in semiconductor production nowadays, and even shorter wavelengths down to the sub-nm rage are under investigation.

The key issue of lithography is the resolution of the system, and hence the size of the smallest feature (minimum feature size: *MFS*) which can be defined on the sample. This *MFS* depends on the illumination method, the illumination wavelength λ, on the materials of the optical system and the resist used. In Sec. 2.1 the different illumination methods and their physical resolution limits are addressed, in Sec. 2.2 the wavelengths and the light sources are discussed, also for wavelengths below 15 nm, while lithography with these wavelengths is discussed in Sec. 3 and 4, and in Sec. 2.3 the materials and the forms of the optical system are dealt with.

2.1 Illumination Methods and Resolution Limits

Figure 3 shows a schematic view of the three different illumination methods *contact, proximity* and *projection lithography*. With all three, the light emitted by a light source passes a condenser optics so that a parallel beam is formed. With contact lithography, mask and sample are pressed together so that the mask is in close contact to the resist (Figure 3a). The resolution is limited by deflection and is expressed by the *MFS* which can be obtained. For contact lithography this is: $MFS = \sqrt{d \cdot \lambda}$, where d is the resist thickness and λ the wavelength. For a resist thickness of 1 µm and a wavelength of about 400 nm, this yields a minimum feature size of 600 nm. The major drawback of this method is that the quality of the mask suffers from contact to the resist, leading to failures in the structure. To avoid this problem, the second method was developed (Figure 3b). With *proximity lithography* there is a defined proximity gap g between sample and mask, so there is no deterioration of the mask. The drawback is the poorer resolution limit, which is proportional to $\sqrt{(d+g)\cdot\lambda}$. With same figures as above and a proximity gap of 10 µm, the *MFS* is 2 µm.

The method used today in industrial production is so-called *projection lithography* (Figure 3c). Here not the shadow of the mask is transferred to the sample as with the two other methods, but a picture of the mask is projected onto the sample. Therefore after passing the mask, the light is bundled by an optical system. The mask is not in contact with the sample, so there is no deterioration as in contact lithography, but the resolution is better than in proximity lithography. Furthermore it is possible to reduce the picture so the patterns on the mask are allowed to be bigger than the patterns on the sample. This is

masks with an accuracy of 100 nm, then the error for a structure of 500 nm to be transferred onto a sample is 20 %, if it is transferred one by one. If the picture is reduced 4 times, then for a 500 nm feature on the sample, the feature on the mask has to be 2 µm; therefore the mask error is only 5 %. Because of the reduction, the wafer is not exposed in one exposure, but in several. This is done by so-called steppers, in which the wafer is adjusted under the mask by an x-y-table. The stepper moves the wafer from one exposure position to the next, while the mask is not moved.

In projection lithography the limiting factor to the MFS is diffraction. Consider a slit width b which is illuminated by a monochromatic plane wave. What will the intensity distribution look like on a screen at a distance l behind the slit? Therefore consider two Huygens waves, one from the lower rim of the slit, one from the middle. There will be an optical path difference between these two Huygens waves, depending on the angle of propagation Θ. The magnitude of the path difference (*PD*) is:

$$PD = \frac{b}{2}\sin(\Theta) \tag{1}$$

The two Huygens waves will interfere destructively if the *PD* is an odd multiple of the half wavelength:

$$\frac{b}{2}\sin(\Theta_{min}) = (2m+1)\cdot\frac{\lambda}{2} \qquad \text{with } m = 0, \pm 1, \pm 2, \ldots \tag{2}$$

Under this condition, the Huygens waves from the lower part of the slit will interfere destructively with the ones from the upper part. At the angle Θ_{min} there is a minimum of intensity.

The Huygens waves do interfere constructively resulting in a maximum of intensity when:

$$\frac{b}{2}\sin(\Theta_{max}) = m\lambda \qquad \text{with } m = 0, \pm 1, \pm 2, \ldots \text{ holds.} \tag{3}$$

In lithography the diffraction patterns of several structures are superimposed so the question leading to the MFS is the question of when two structures can be resolved. The first approach is given by the Rayleigh criterion [3]. When light coming from a point source passes an optical system a blurred diffraction pattern – the Airy disc – occurs. The Rayleigh criterion says that two ideal point sources (e.g. stars) can be resolved when the intensity maximum of the one Airy disc is in the first minimum of the other, so *MFS* is given as:

$$MFS = 0.61\cdot\frac{\lambda}{NA} \tag{4}$$

where *NA* is the numerical aperture of the optical system. Nevertheless the Rayleigh criterion is just a first approach to the *MFS* in microlithography. The mask patterns are not independent (i.e. incoherent) ideal point sources, on the contrary they have a finite width and the light is partially coherent. Nevertheless, the form of the criterion gives the right dependences. If the wavelength is decreased by 10 % or the *NA* is increased by 10 %, the *MFS* is improved by 10 %. Furthermore, it was derived only by properties of the optics although the photoresist also affects the MFS. Therefore more generally, the criterion is written as:

$$MFS = k_1\cdot\frac{\lambda}{NA} \tag{5}$$

where k_1 is a constant (typically 0.5 – 0.9), which accounts for non-ideal behaviour of the equipment (e.g. lens errors) and the influences which do not come from the optics (resist, resist processing, shape of the imaged structures,...). Therefore k_1 is called the technology constant.

As a comparison, for a technology constant of 0.7 and a numerical aperture of 0.7, which are commonly used figures, the *MFS* is in the order of the wavelength λ. So it is better by about a factor of 0.66 than the *MFS* of contact printing.

Risoluzione spaziale III

Figure 4 clarifies the connection between mask, diffraction and intensity distribution in the image plane. Due to diffraction two sharp features, P and Q, on the mask give rise to an overall intensity distribution on the sample. To resolve these two features the intensity distribution has to have a minimum between the two main maximums. It is useful to define the so called modulation transfer function (*MTF*) as:

$$MTF = \frac{I_{max} - I_{min}}{I_{max} + I_{min}} \qquad (6)$$

The higher the value – the higher the difference between the maximum and minimum intensity – the better the contrast between exposed and unexposed areas, the better is the resolution of the equipment. It should be noted that the *MTF* is only derived by properties of the optical system. It is a measure of the capabilities of the lithographic tool in printing structures.

Contrasto del pattern impressionato è limitato dal fenomeno della diffrazione

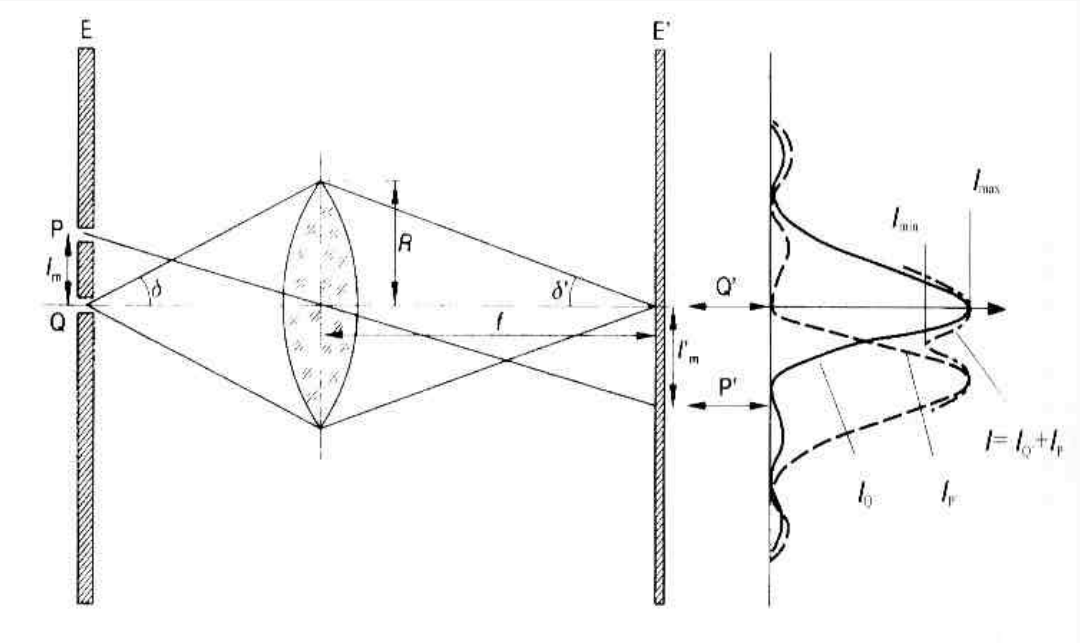

Da R. Waser Ed., Nanoelectronics and information technology (Wiley-VCH, 2003)

Strategie di aumento risoluzione: phase shift masks

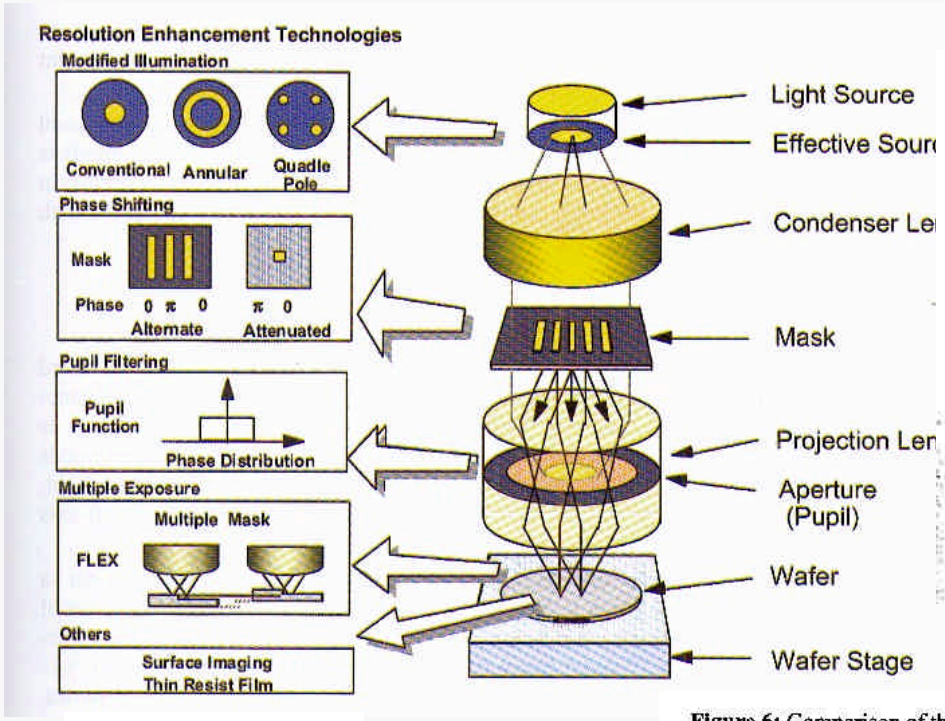

Figure 5: Survey of the resolution enhancement techniques.

so-called *Levenson* or *alternating phase shift masks* (PSM) can improve the resolution by 40 %. Unfortunately, this improvement is pattern-dependent; for a single structure there is no neighboring structure, so there is no light to interfere with. Even if there are structures which are not in a regular arrangement, there is no defined phase shift between these structures which could yield an improvement in the resolution of all structures.

The phase shift can be obtained by an additional transparent layer on the mask. If it has the refractive index n and thickness d, the phase shift is $\Phi = (n-1)2\pi d/\lambda$. So a shift of π is obtained, when the condition $d = \lambda/[2(n-1)]$ holds. On the other hand, it is also possible to recess the mask material so that the right optical path difference is obtained. But the etch depth can be controlled by the time only, and not, as in etching away an additional layer, by the thickness of the layer itself.

To deal with the drawbacks of alternating PSM, several other methods have been developed, which are described next. In rim-PSM, the whole mask is covered by a phase-shifter material and then with the resist. After development, the phase shifter is etched anisotropically and the masking layer is etched isotropically. By this a undercut under the phase shifter occurs at the rim of every structure. This also yields a resolution improvement, but not as much as with alternating PSM, although it is therefore not limited to certain structures.

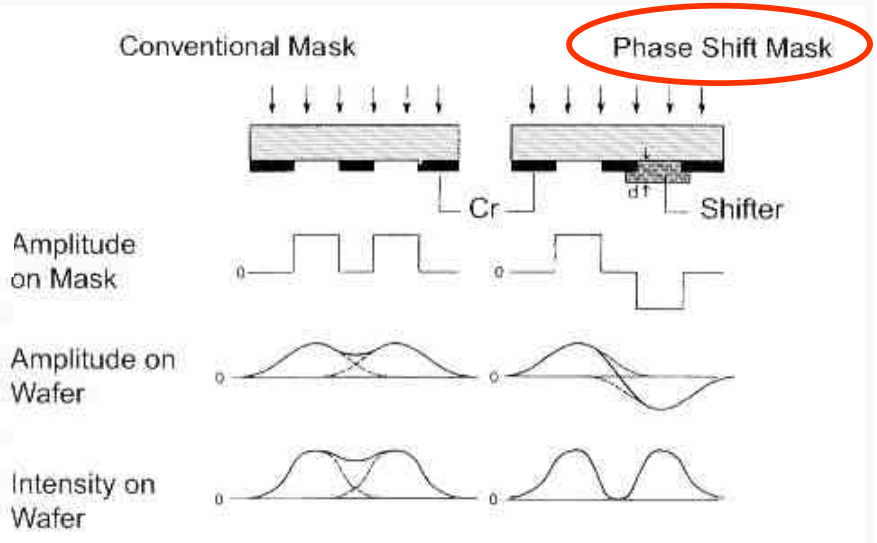

Figure 6: Comparison of the light amplitudes and intensities at the mask and on the wafer for a conventional and a phase shift mask. Note that the intensity on the wafer between the two features is zero for the phase shift mask [26].

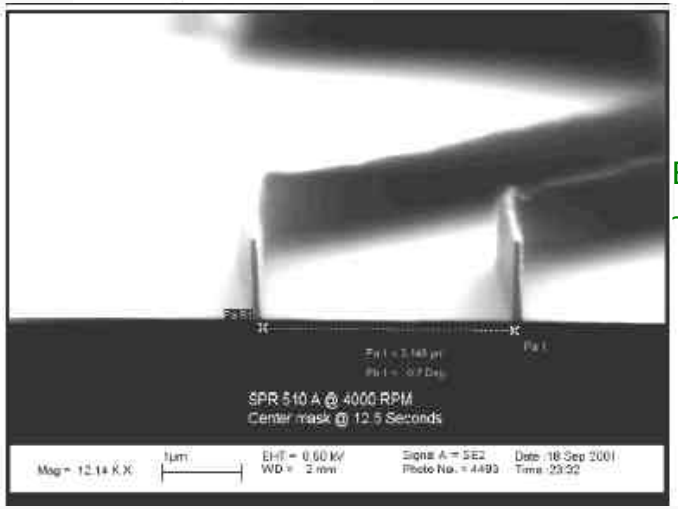

Esempio: features ~ 100 nm ottenute con sorgenti luce da 350 nm

Strategie di aumento risoluzione: off axis illumination

Off-Axis Illumination

To improve resolution without decreasing the wavelength or increasing *NA*, so-called off-axis illumination was applied. The method was already known as a contrast-enhancing technique for optical microscopes. With off-axis illumination, the light beam is directed from the mask towards the edge of the projection lens, and not, as in on-axis illumination, towards the center. In normal illumination with partially coherent light, there always is part of the light which is off-axis, but in the context here with off-axis illumination there is no on-axis component.

To understand the mode of operation of off-axis illumination, consider a line-and-spaces structure with pitch p. The incident light will be diffracted into a set of beams, of which only the undiffracted beam, the zero-order beam, travels in the direction of the incident light. The 1st order beam travels under the angle $|\theta_1| = \arcsin(\lambda / p)$. If p is too small, then $|\theta_{+1}|$ is bigger than the acceptance angle α of the projection optics, then only the zero-order beam is projected to the sample (Figure 7a). But this does not carry any information of the pattern, and hence the pattern cannot be transferred onto the sample. At least the zero- and the 1st order beam have to be in the range of the aperture angle. If the incident light hits the mask under an angle $\Theta_0 < \alpha$ the undiffracted beam enters the projection lens at the edge, and the 1st order beam is still collected by the lens, and therefore a pattern transfer is still possible. The angle of incidence Θ_0 can be realized by inserting an aperture in the optical path between condenser and mask (Figure 7b).

Although the higher resolution is an advantage of off-axis illumination, the impact on the depth of focus (DOF) is of even greater value. In on-axis illumination, the beams of different deflection orders have to travel in different ways so they are phase-shifted to each other, which results in a lack of focus. In off-axis illumination, the zero order and 1st order beam reaches the projection lens at the same distance from the center, which means that their optical path length is the same. So the relative phase difference between these beams is zero, which increases the DOF dramatically.

Off-axis illumination is facilitated by an aperture (Figure 8) which is located in front of the condenser lens. It depends on the apertures shape which structures are improved. If there is an aperture as in Figure 8a, only the structures perpendicular to the arrangement of the apertures will be improved. The aperture shown in Figure 8b yields an improvement of structures which are adjusted to *good* angles – up/down or left/right direction. This is sufficient because in normal cases, the features are in a *good* arrangement. The aperture in Figure 8c even decreases this problem, but here the improvement in DOF is less.

When the resolution in principle has to be improved, then according to the Rayleigh criterion either the wavelength λ or the technology parameter k_1 have to be decreased, or the numerical aperture *NA* has to be increased.

Increasing *NA* means physically bigger lenses. Here the problem arises that it is difficult to produce huge lenses with the required quality; on the other hand the available materials also limit the physical size of the lenses. So there are still two possibilities of increasing the resolution: smaller λ and smaller k_1.

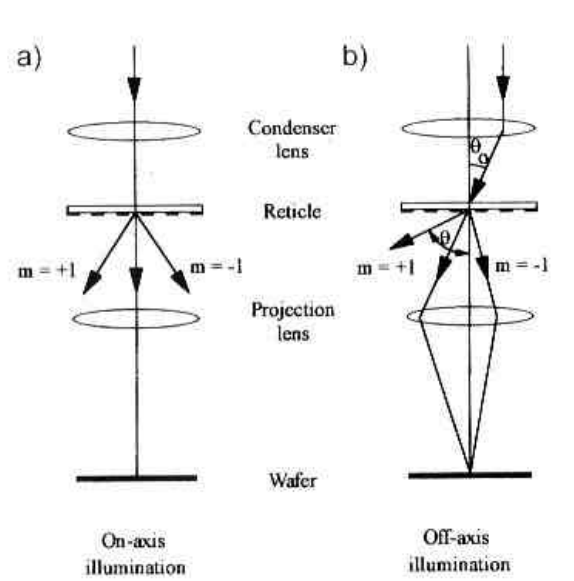

Figure 7:
(a) Optical path and deflection orders of on-axis and
(b) off-axis illumination. Note that with the same wavelength and structure size, the off-axis illumination allows the 1st order beam to pass the optical system [3]. A good description of off-axis illumination is also found in [6].

Numerose tecniche permettono di avvicinare (e un po' superare??) il limite di diffrazione

Diligenti et al.
APL 75 489 (1999)

Strategie di aumento risoluzione: etching anisotropo

An (110) silicon substrate (p doped, resistivity $=1-10\,\Omega\times$cm) was oxidized (1050 °C for 30 min) to obtain a 350 nm SiO_2 layer. Standard photolithography was employed to pattern the oxide; the mask used is shown in Fig. 1(a). It consisted of an array of lines (width 4 μm, length 3000 μm, spacing 4 μm) which must be aligned along the $[\bar{1}12]$ direction. After the oxide definition, an anisotropic etching was performed by means of an ethylenediamine-pyrocatechol (EDP) solution type F (fast) at 115 °C.[16] After 1 h of etching walls with an high aspect ratio [Fig. 1(b)] (height=35 μm, width in the range 1–4 μm, depending on the alignment accuracy along the $[\bar{1}12]$ direction) were obtained. For samples with a misalignment greater than 0.07 degrees there was a complete underetching of the planes.[17] Each array contained 1000 planes; Fig. 2 (top panel) shows a scanning electron microscope (SEM) micrograph of a cross section of an array of planes.

The samples were then etched in buffered HF (BHF) to remove the oxide mask layer indicated as SiO_2 in Fig. 1(b), and underwent a oxidation. The sequence of oxidation/etching steps allowed to reduce the wall thickness in a controlled way, and PL measurements were carried out after each step to investigate the dependence of the emission features on the wall width. Figure 2 (bottom panel) is a closer view of a cross section of the planes, which shows that the Si core thickness is not uniform, an effect probably due to a minor oxygen diffusion at the bottom of the walls.

Etching anisotropo + ossidazioni successive
--> aumento risoluzione spaziale

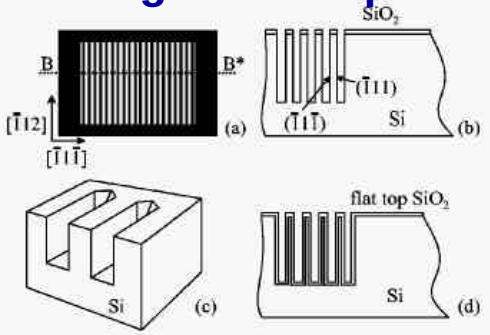

Mask alignment

FIG. 1. Schematic view and orientation of the mask (a); result of the EDP etching (cross section along the line BB*) (b); a perspective view of the planes at the end of the etched zone (c); the two zones, flat top and array, where the PL was investigated (d).

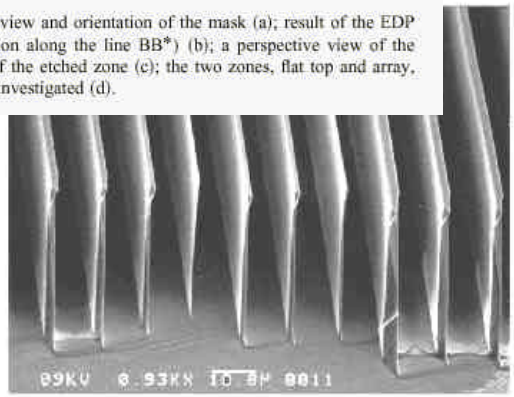

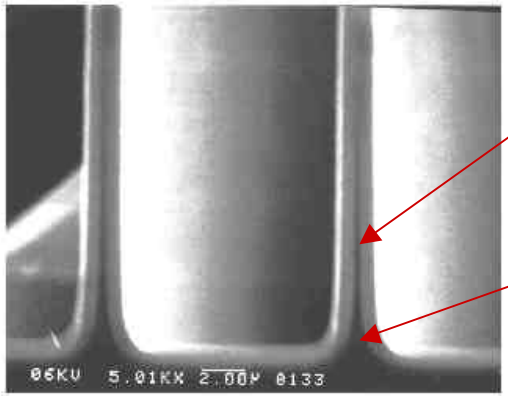

ossido

Si-cristallino

FIG. 2. SEM view of the array cross section (top panel); a closer view showing the oxidation effect (bottom panel).

Side-wall patterning

Processo di fabbricazione “complesso”
(ma economico!!) per creare Si-nanowires:

a) ossidazione dry (spess. 0.5 µm):
$Si\ (s) + O_2 \rightarrow SiO_2$
seguita da deposizione Si_3N_4 e patterning via lito. ottica convenzionale
b) CVD poly-Si (pirolisi SiH_4 a bassa p):
SiH_4 + calore(T~1100 °C) $\rightarrow$ Si (s) +2 H_2 (g)
c) Reactive Ion Etching del poly-Si con fascio ionico “inclinato”
--> rimane poly-Si solo sui bordi
d) wet chemical etching selettivo
(soprattutto nitruro) con H_3PO_4
e) rimozione ossido (poly-Si funge da maschera) con etching selettivo
f) rimozione nitruro con RIE non inclinata

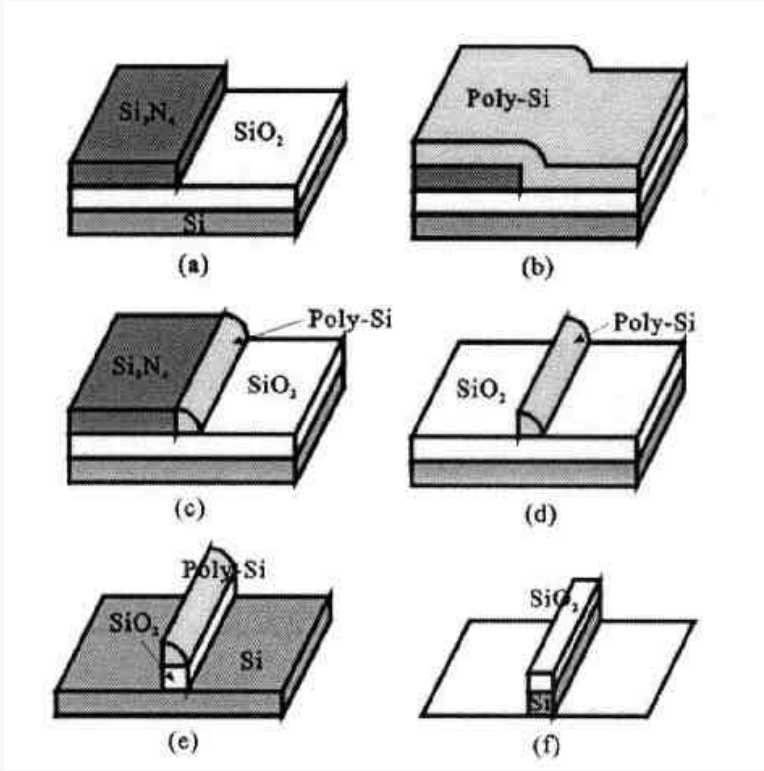

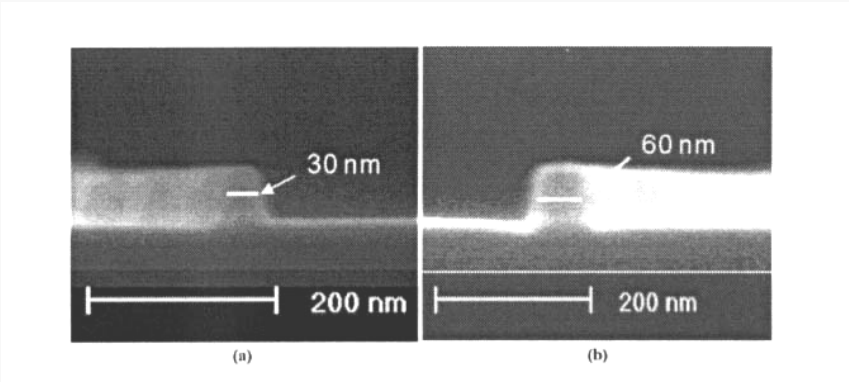

SEM cross sections (in “prospettiva”)

Risultati competitivi (su silicio!) con tecniche più sofisticate (es. EBL)

Sorgenti di luce a bassa lunghezza d'onda

Wavelength [nm]	Source	Range
436	Hg arc lamp	G-line
405	Hg arc lamp	H-line
365	Hg arc lamp	I-line
248	Hg/Xe arc lamp; KrF excimer laser	Deep UV (DUV)
193	ArF excimer laser	DUV
157	F_2 laser	Vacuum UV (VUV)
~10	Laser-produced plasma sources	Extreme UV (EUV)
~1	X-ray tube; synchrotron	X-ray

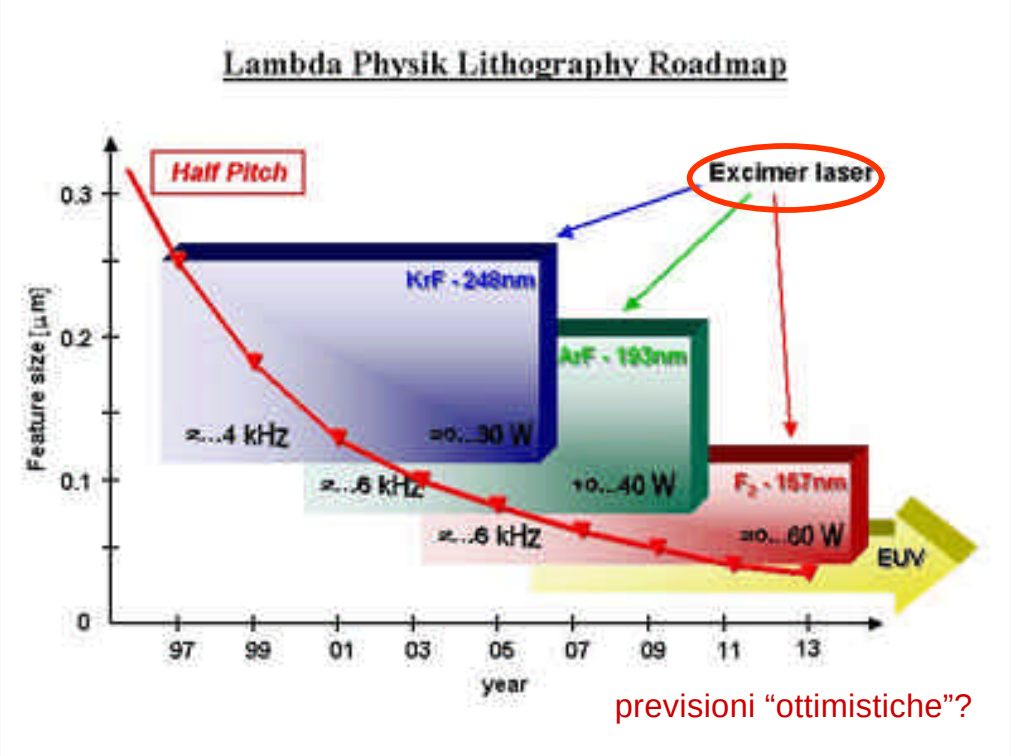

previsioni "ottimistiche"?

Sviluppo continuo (??) di sorgenti laser a lunghezza d'onda sempre minore (ed elevata "funzionalità")

X-Ray lithography (XRL)

Sorgente “ottimale”: sincrotrone
(fascio intenso e ben collimato)
--> proximity mode masks

Resist: typ. PMMA
(sensibilità critica
--> alte dosi, ~ 2 J/cm^2)

Problema: fasci di elettroni
generati da scattering
X-Rays su mask, resist, subs...

Risoluzione effettiva
~ decine di nm

Vantaggio: profondità di campo (fascio collimato)
--> high aspect ratio features, LIGA,...

Da M. Madou,
Fundamentals of microfab.,
CRC (1997)

Maschere:
typ. membrane Si

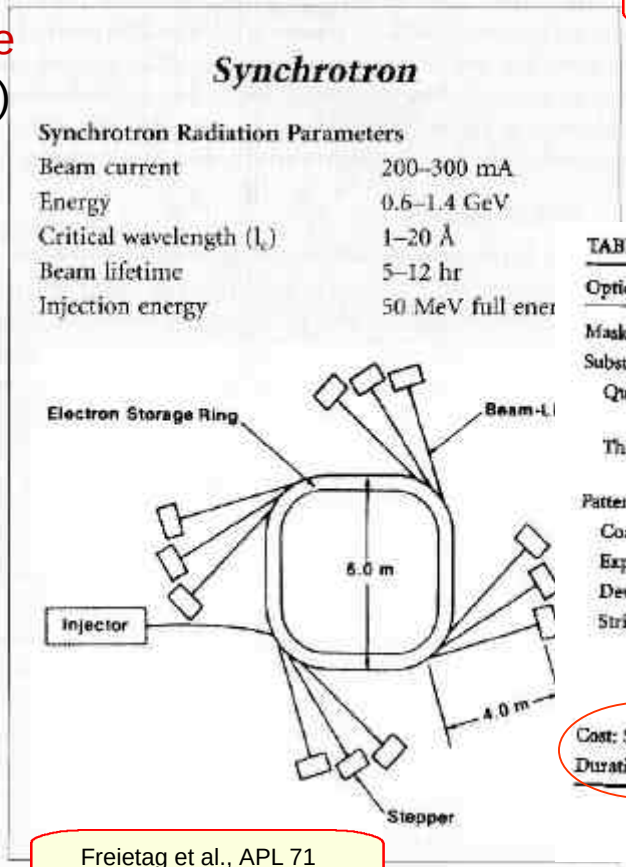

TABLE 1.5 Optical vs. X-Ray Mask

Optical Mask	X-Ray Mask
Mask design: CAD	Mask design: CAD
Substrate preparation	Substrate preparation
Quartz	Thin membrane substrate (Si, Be, Ti, ...)
Thin metal film deposition	Deposit plating base (50 Å Cr, then 300 Å Au)
Pattern delineation	Pattern delineation
Coat substrate with resist	Coat with resist
Expose pattern (optical, e-beam)	Expose pattern (optical, e-beam)
Develop pattern etch Cr layer	Develop pattern
Strip resist	Absorber definition:
	Electroplate Au (~15 μm for hard X-rays)
	Strip resist
Cost: $1K–$3K	Cost: $4K–$12K
Duration: 3 days	Duration: 10 days

Freietag et al., APL 71
1441 (1997)

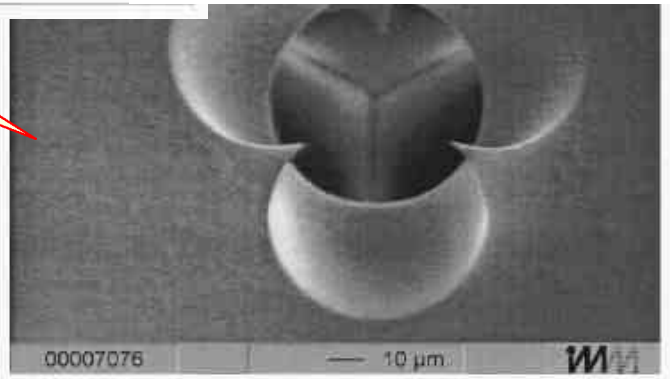

FIG. 2. Intersection of three holes in a photonic crystal made from positive tone resist.

Limiti XRL

4 X-Ray Lithography

Decreasing the wavelength even further into the x-ray range yields so-called x-ra lithography. For these short wavelengths it is not possible to set up an optical path nei ther in reflection optics nor in refraction optics. On one hand, there is no material whicl is transparent enough to make lenses or masks from, and, on the other hand, it is not pos sible to make Bragg-reflectors. The individual layers in the layer stack have to have thickness of $\lambda/4$, which corresponds to a layer thickness of ~0.3 nm. This is in the rang of the thickness of one monolayer and is not achievable..

Projection x-ray-lithography is therefore not possible, but proximity x-ray lithogra phy (PXL) is possible. The advantages are the high resolution limit ($\sim\sqrt{\lambda\cdot(g+d)}$ which is about 30 nm for 1 nm exposure wavelength) and the insensitivity to organi contamination. These contaminations (as all low atomic number materials) do no absorb the x-rays, and hence are not printed onto the sample.

But there are some limitations. Consider a source with diameter a of 1 mm at dis tance L of 1 m towards the mask and a proximity gap g of 10 µm. Then there is th so-called *penumbral blur* $\xi = a \cdot g / L \sim 10$ nm, which limits the resolution (Figure 16) Furthermore, the pattern is not transferred correctly to the sample. Even if a point sourc is used, there is a displacement Δ of $\Delta = r \cdot g / L$, where r is the radial position on th sample (Figure 16). This error can be eliminated if it is taken into account when th mask pattern is generated.

Nevertheless, if synchrotron radiation is used, a high intense beam of parallel ligh is available so these errors do not occur. This parallel beam has another advantage: Du to the small deflection the exposure shows a high depth of focus of several µm, facilitat ing exposures of textured substrates or of thick resists (Figure 17).

The problem for PXL is the masks. Since there is no material which is as transpar ent to x-ray as quartz to DUV, the carrier layer has to be thin (1 – 2 µm). On the othe hand, there is also no material which is as opaque to x-ray as chromium to DUV, so th masking layer has to be thick enough (300 – 500 nm). A carrier layer of 1 µm SiC onl has a transparency of 57 %, while a masking layer of Au still lets 14 % of the light pass The absorbed light will heat the mask so that it expands, which leads to another uncer tainty in the pattern transfer. Furthermore, PXL is a non-reduction printing method, s the features on the mask are of the same size as on the sample. This makes the produc tion of the masks very complicated when the target ist the sub-100 nm range.

The mask production sequence is as follows: On a silicon wafer, a thin membran layer is deposited (e.g. SiC, Si_3N_4). Onto this layer, a chromium etch stop layer and th masking layer of 300 – 500 nm of a high-atomic number material is evaporated (e.g. Au Ta). Then the mask is coated with an e-beam resist and exposed in an e-beam direct-write system. The resist is used to etch the masking layer with an etch stop on th chromium so the membrane is not hurt.

The commonly used DUV resists show good process aptitude.

Proximity mask

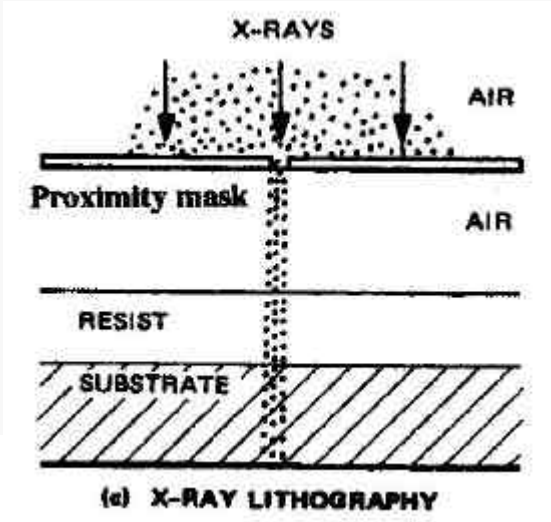

Mask materials

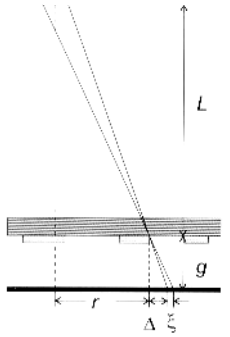

Penumbral blur

Figure 16: Penumbral blur ξ and displacement error Δ for proximity x-ray lithography. L is the distance from source to mask, g is the proximity gap and a is the lateral diameter of the source [11].

Litografia atomica

See
http://nanocold.df.unipi.it

Idea di base:

fascio di particelle neutre al posto di radiazione e.m.

--> diffrazione a livello sub-nm (λ_{dB}) *senza problemi dei fasci di cariche*

Vantaggi ulteriori:

- uso di “maschere ottiche” (non invasive, species-selective,…)
- possibilità deposizione diretta (bottoms-up a livello atomico) o resist-assisted
- carattere “parallelo” della tecnica mantenuto come in lito. ottica

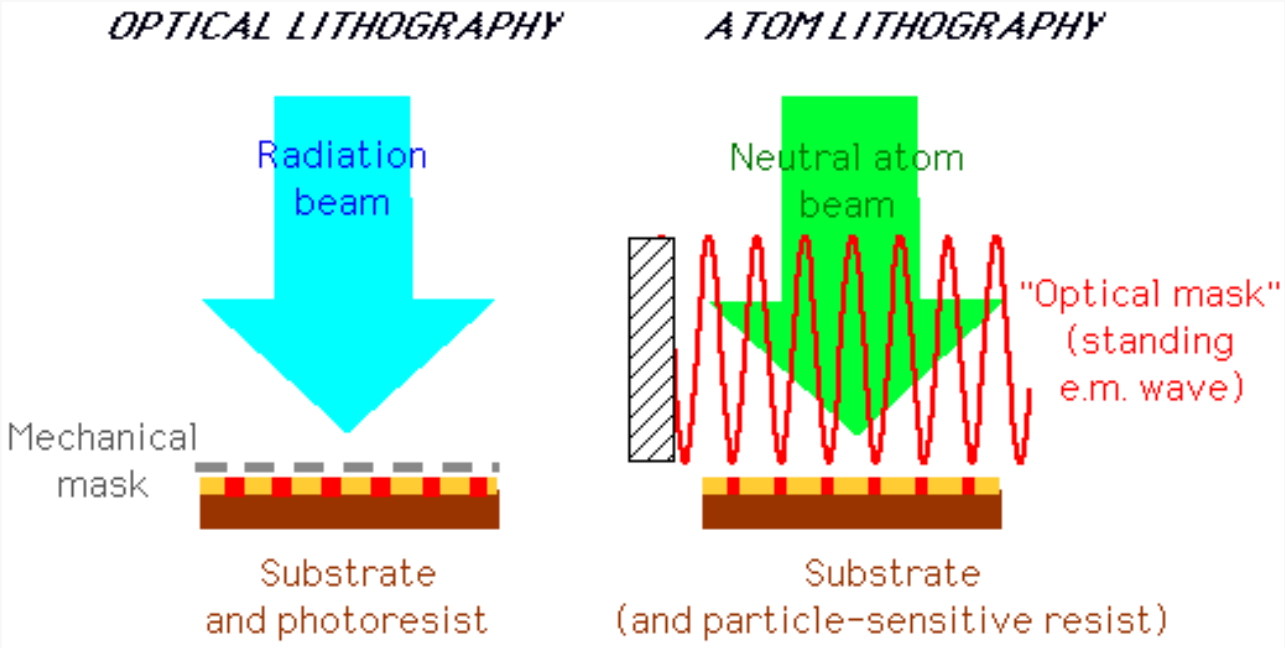

Ingrediente fondamentale:
capacità di manipolare la dinamica di atomi neutri (atom-optics <-- laser cooling)

Cenni di atom optics

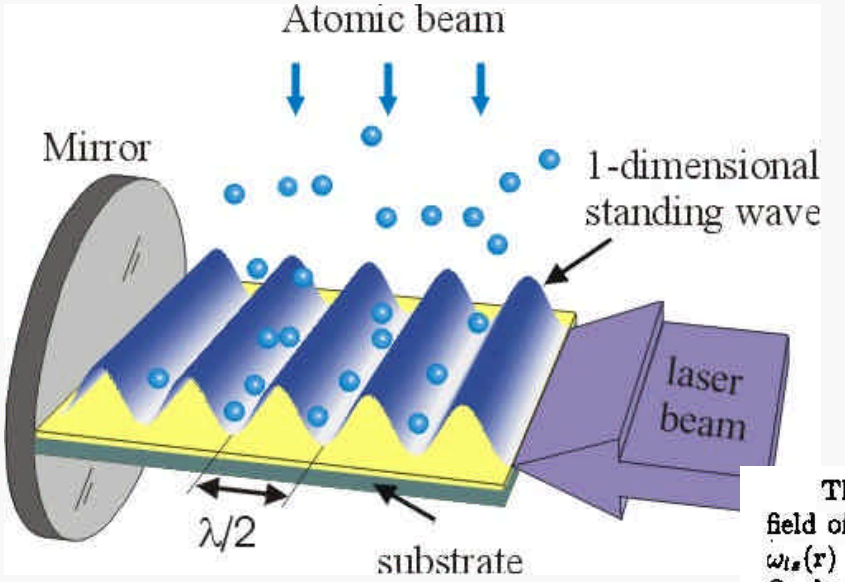

Maschera ottica: onda stazionaria
--> forza “dipolare” (conservativa)
in direzione trasversa al moto degli atomi (per opportuna scelta della frequenza, prossima a ris. atomica)

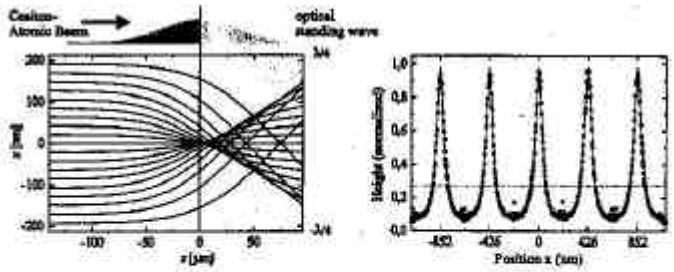

Figure 3. *Left: Numerically calculated trajectories of a laser cooled beam of atoms focussed to the center of a Gaussian envelope standing wave light field (thick lens limit). The focussed laser beam forming the optical standing wave is clipped by the substrate. Note the different scales in x- and z-directions. Right: Analysis [25] of flux concentration for a realistic beam of thermal cesium atoms with 0.1 m/s transversal rms velocity at the focal plane z=0. The dotted line shows the flux distribution without the standing optical wave.*

Meschede Metcalf in press (2002)

The optical dipole force acting on an atom with resonance frequency ω_A in a laser field of detuning $\delta = \omega_L - \omega_A$ is derived from the spatial variation of the light shift $\omega_{ls}(r)$ [1]. For a single laser beam travelling in the x-direction with Rabi frequency Ω, the light shift is given by

$$\omega_{ls} = \left[\sqrt{\Omega^2 + \delta^2} - \delta\right]/2 \,. \qquad (1)$$

For sufficiently large detuning $\delta \gg \Omega$, approximation of Eq. 1 leads to $\omega_{ls} \approx \Omega^2/4\delta = \gamma^2 s/8\delta$, where $s \equiv I/I_{sat}$, I is the laser beam intensity, $I_{sat} \equiv \pi hc/3\lambda^3\tau$ is the saturation intensity, and $\tau \equiv 1/\gamma$ is the atomic excited state lifetime.

In a standing wave with $\delta \gg \Omega$, $\omega_{ls} = \omega_{ls}(x)$ varies sinusoidally from node to antinode and also spontaneous emission is inhibited so that $\hbar\omega_{ls}(x)$ may be treated as a potential $U(x)$. The resulting dipole force is

$$\mathbf{F}(x) = -\nabla U(x) = -\frac{\hbar\gamma^2}{8\delta I_{sat}} \nabla I(x) \equiv U_{max} \nabla f(x), \qquad (2)$$

where $I(x) = I_{max} f(x)$ is the total intensity distribution of the standing wave light field of period $\lambda/2$, I_{max} is the maximum intensity, and $f(x)$ describes the normalized modulation of the light field. For such a standing wave, the optical electric field (and the Rabi frequency) at the antinodes is double that of each travelling wave that composes it, and so the total intensity I_{max} at the antinodes is four times that of the single travelling wave.

Onda stazionaria
--> array di nanolenti atomiche

Requisiti su fascio atomico

1. Intensità --> tempi di esposizione “ragionevoli”

2. Collimazione --> efficacia focalizzazione
   (array di nanolenti ~ array di buche pot.)

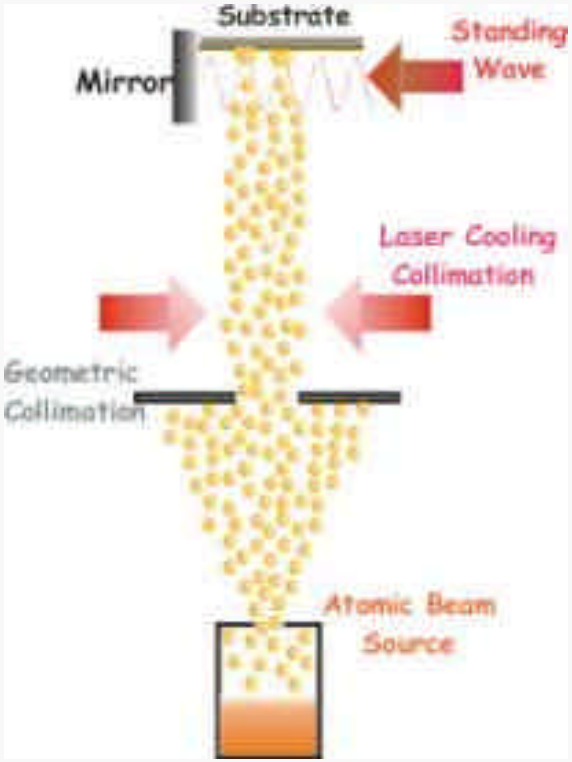

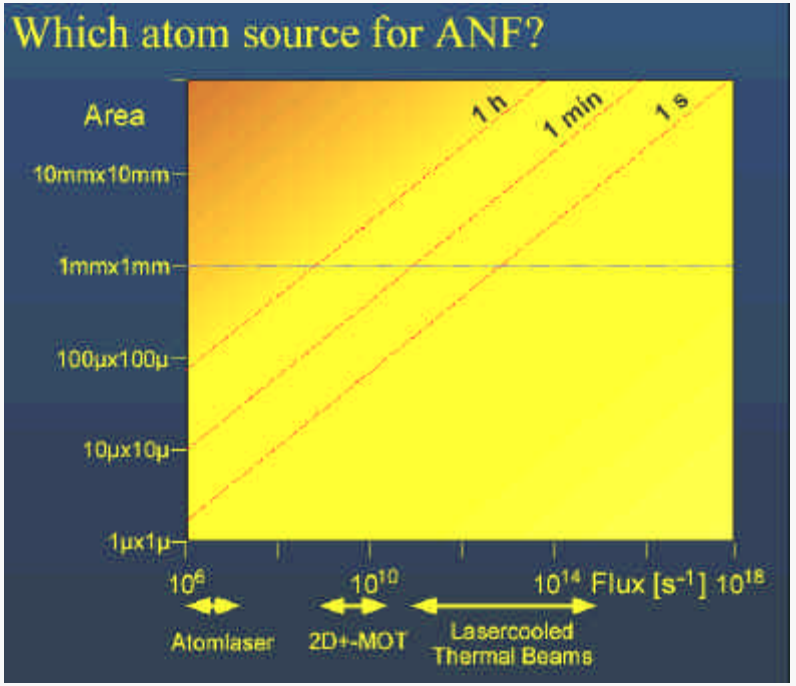

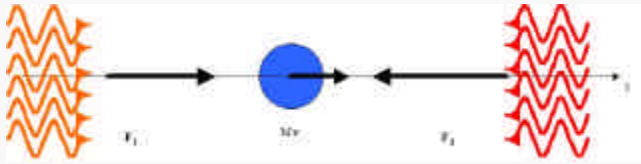

Melassa ottica

$$F = F_1 - F_2 \approx 4v(\omega - \omega_{12})\hbar k^2 \langle n_{sp} \rangle \frac{1}{(\Gamma_s/2)^2 + (\omega - \omega_{12})^2} \equiv -M\gamma v$$

Tecniche di laser cooling usate per aumentare collimazione e intensità fascio atomico

Applicabilità litografia atomica

Attualmente si applica a specie che possono essere manipolate facilmente via laser (lunghezza d'onda, intensità, *schemi "chiusi"* di raffreddamento laser,…)

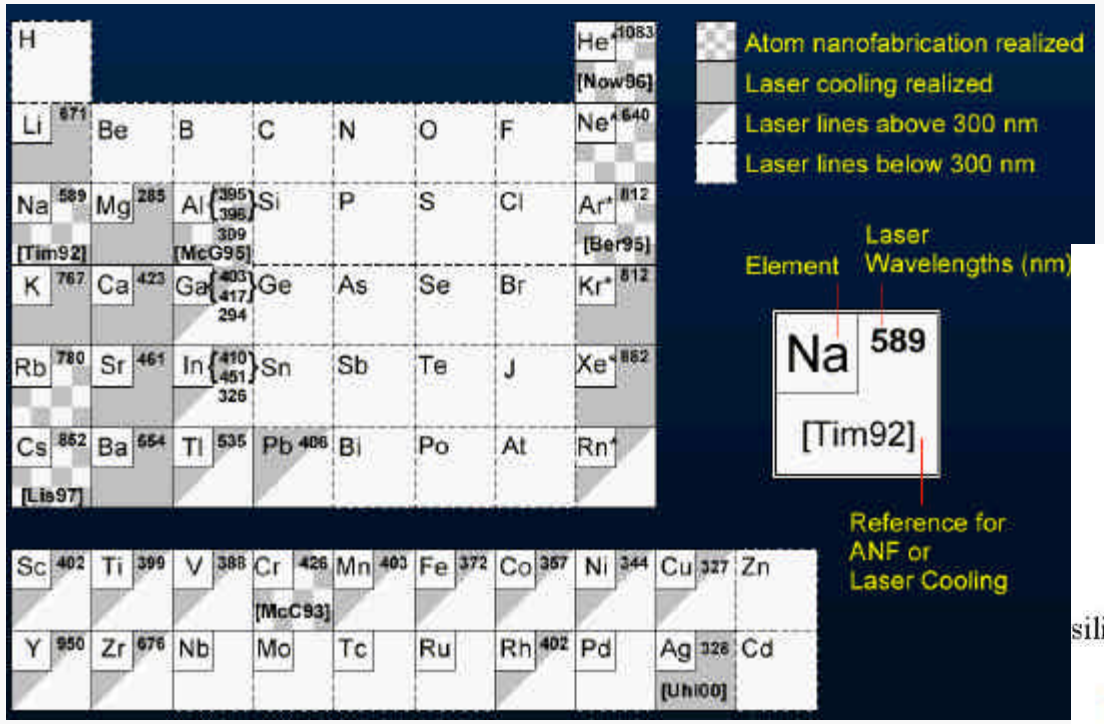

Atom	T_S K	λ nm	γ 10^7/s	v_c m/s	ϑ_c mrad	S/ω_r μs	$2r_c$ mm	P_c mW	Θ_D mrad	Θ_R mrad	P_{ANF} mW
$^4He^*$	300	1083	1.0	1.7	1.5	19	0.03	0.03	0.36	0.11	0.40
^{23}Na	630	589	6.2	5.8	13	32	0.18	1.0	0.89	0.09	0.12
^{27}Al	1640	309	8.2	4.0	4.0	10	0.04	6	0.44	0.07	0.95
$^{40}Ar^*$	300	812	3.6	4.8	17	105	0.49	0.5	0.68	0.05	0.15
^{52}Cr	1825	426	3.1	2.1	3.5	37	0.08	2.4	0.26	0.03	2.0
^{56}Fe	1920	372	1.6	1.0	1.3	31	0.03	1.5	0.18	0.04	4.6
^{70}Ga	1555	403	4.9	3.1	5.2	45	0.14	4.3	0.35	0.03	1.1
		417	9.2	6.1	10	48	0.29	7.8	0.48	0.03	0.59
^{109}Ag	1435	328	1.4	7.2	15	46	0.33	18	0.61	0.03	0.46
^{115}In	1355	410	5.8	3.8	8.5	77	0.29	5.0	0.40	0.03	0.83
		451	10.2	7.3	16	93	0.68	9.5	0.54	0.02	0.43
^{133}Cs	410	852	3.3	4.5	20	383	1.7	3.3	0.55	0.02	0.21
^{197}Au	1800	268	16.7	7.1	19	57	0.40	32	0.59	0.04	0.60

Per elementi reattivi in aria
(es. alcalini)
--> resist-assisted (SAM)

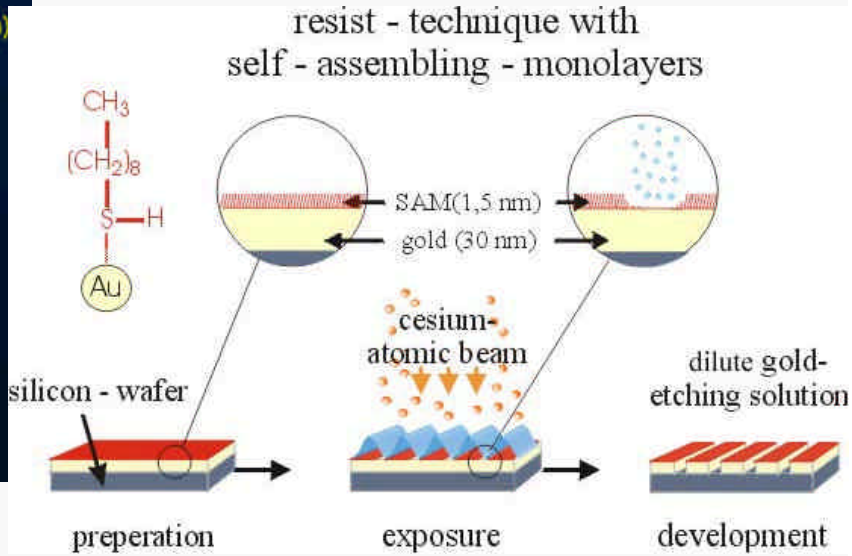

Svantaggio litografia atomica:
scarsa flessibilità
(dipende anche da sviluppo nuovi laser)

Alcuni esempi di litografia atomica

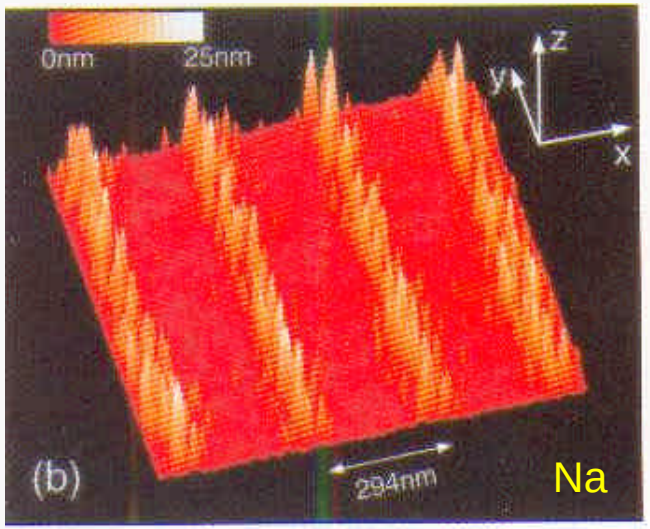

Timp et al. PRL 69 1636 (1992)

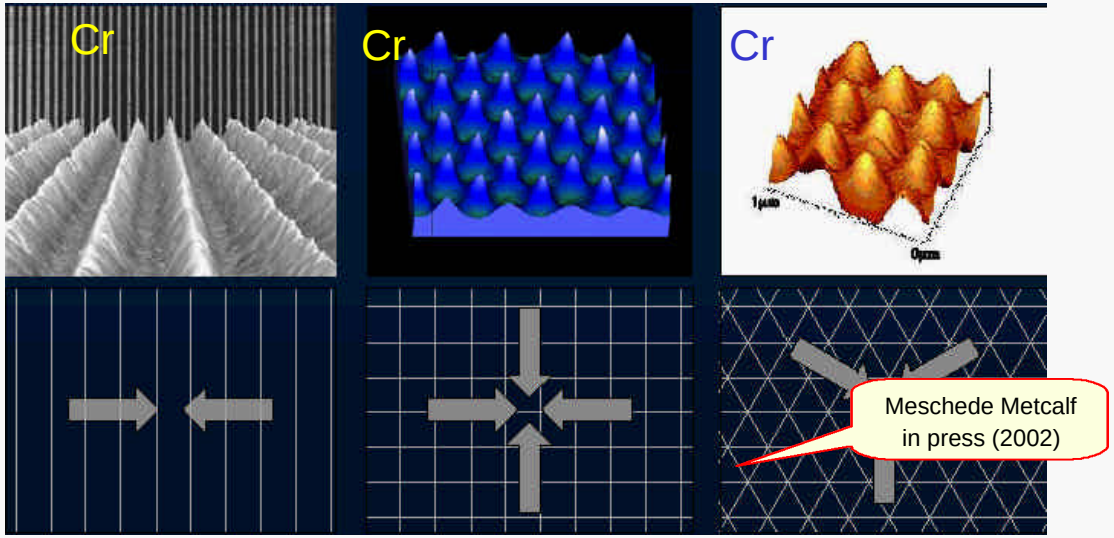

Onda stazionaria 1D

McClelland et al.
Science 87 262 (1993)

Onde stazionarie 2D

Gupta et al.
APL 67 1378 (1995)

Drodofsky et al.
Appl Phys B 65 755 (1997)

Holographic lithography

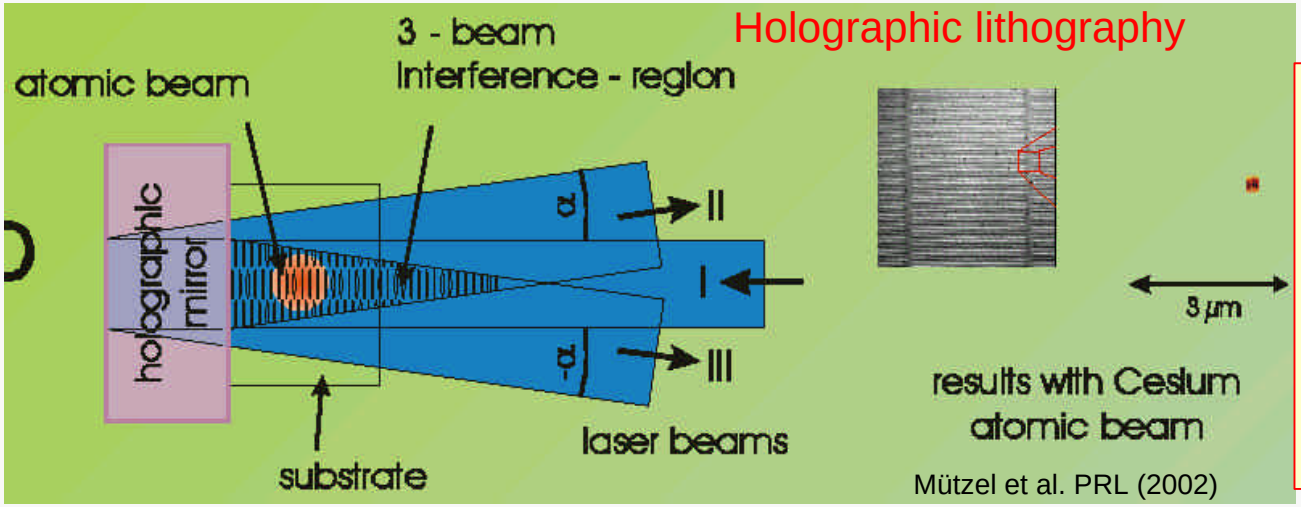

Mützel et al. PRL (2002)

Vantaggio/svantaggio:
regolarità interferometrica
nanostrutture
(ma esistono “rimedi”)

Risoluzione max:
~ 15-20 nm (*finora!!)*

Nanoimprinting per hot embossing

9 Nanoimprint Lithography

There are several approaches for patterning structures without lithographic methods, e.g. a silicon surface can be modified by depassivation by the tunneling current in a UHV-STM (Ultra High Vacuum Scanning Tunneling Microscope [20], [21], or the surface can be modified by the movement of an Atomic Force Microscope (AFM)-tip . A certain interest has been focused on the nanoimprint lithography (NIL), which is described in more detail in this section.

With the NIL a mold is processed by conventional technology, i.e. e-beam lithography and etching techniques, and is pressed onto a resist coated substrate. The structures in the mold are transferred into the resist and can be utilized after removing the mold. There are two different kinds of NIL, the hot embossing technique and a UV-based technique. A sketch of both techniques is given in Figure 29.

Hot Embossing Technique

Here the sample is heated above the glass transition temperature of the resist, which is a thermoplastic polymer. Above that temperature the polymer behaves as a vicous liquid and can flow under pressure. The mold itself can be made of different materials, usually a silicon wafer with a thick SiO_2 layer is used. This SiO_2 layer is patterned and structured by e-beam lithography and anisotropic reactive ion etching. The aspect ratio of the features are 3:1 to 6:1, and the mold size is several cm^2. As thermoplastic polymers either PMMA (a well known e-beam resist) or novolak resin-based resists are in use. PMMA has a small thermal expansion coefficient of $\sim 5\times10^{-5}\,K^{-1}$ and a small pressure shrinkage coefficient of $\sim 3.8\times10^{-7}\,psi^{-1}$. To ensure a proper removal of the mold, the resist is modified by release agents, which decrease the adhesion between mold and resist. Resist layers between 50 and 250 nm thickness are used. The imprint temperature and pressure are dependent on the resist. For PMMA the glass transition temperature is about 105°C, so the temperature at which the sample and the mold are heated is between 140 and 180°C. Then the mold is pressed onto the sample with pressures of about 40 – 130 bar. The temperature is then lowered below the glass transition temperature and the mold is removed. The features of the mold are now imprinted in the resist. The residual resist layer in these features is removed by anisotropic reactive ion etching. Afterwards, the structures can be transferred to the substrate either by direct etching or by metal deposition and lift-off. Structures down to a feature size of 10 nm for holes and 45 nm for mesas are imprinted with a high accuracy [22]–[24].

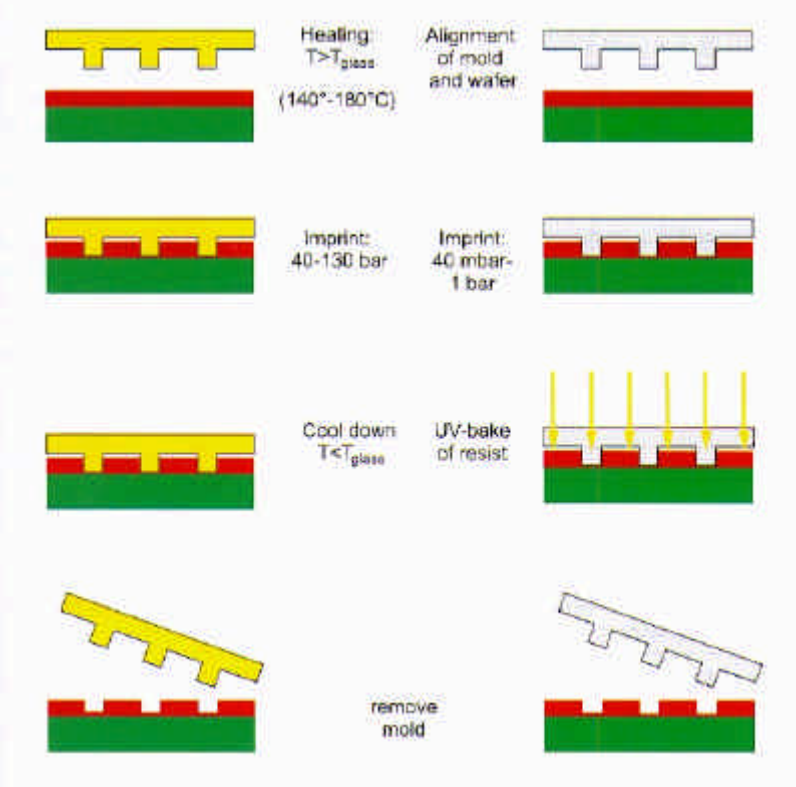

"Replicazione" di nanostrutture da matrice per via termomeccanica

Nanoimprinting per radiazione UV

UV-based NIL

Heating and cooling of mold and sample is time-consuming. Therefore to achieve a somehow higher throughput, curing of the resist by UV irradiation is used. The thermoplastic resist is replaced by UV-curable monomers. The mold has to be fabricated of a UV-transparent material, e.g. quartz. The features are transferred to the mold by e-beam lithography and a Ti/PMMA resist stack. The patterned PMMA is used to transfer the features into the Ti, and the Ti is used to structure the quartz mold. The resists are acrylate- or epoxide-material systems, which can be modified with respect to low viscosity, UV curability, adhesion to the substrate and detachment from the mold. The low viscosity is essential for using low imprint pressures of 40 mbar – 1 bar. After pressing the mold on the sample, the sample is irradiated by UV-radiation through the mold and a baking, and hence a polymerization of the resist is initiated. This step lasts only about 90 seconds. After detaching the mold, the residual resist is removed by RIE and the further pattern transfer can be done. Again mold areas of several square centimeters can be imprinted in one run, and one imprint step takes about 10 minutes. The minimum feature size reported in the literature is 80 nm for dots. [25].

NIL offers the opportunity to define decananometer features in a rather *simple* manner, at least in comparison to the advanced lithography methods described above. The field size of ~2×2 cm^2 is comparable to a die which is illuminated by a stepper. On the other hand, this method is time-consuming (>10 min for one imprint) and up to now only structures on a plain surface have been investigated, while advanced lithography is able to define structures on textured substrates. Nevertheless, because of its technological simplicity, the NIL will be an alternative for research and small series production.

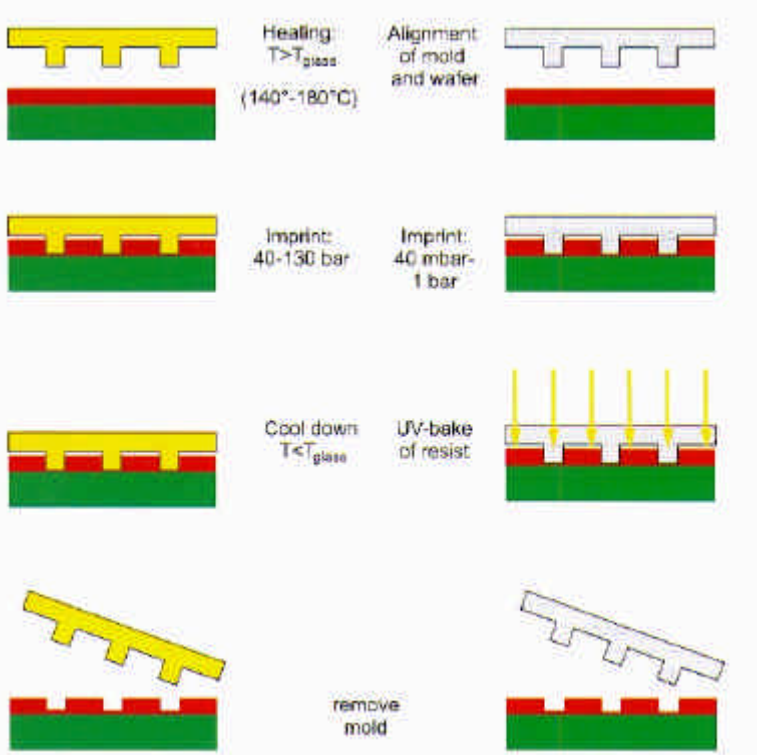

Figure 29: Nanoimprint lithography: hot embossing technique (left hand side) and UV nanoimprint (right hand side).

"Replicazione" di nanostrutture da matrice per via meccanica attivata da UV